Winter Arctic sea ice thickness from ICESat-2: upgrades to freeboard and snow loading estimates and an assessment of the first three winters of data collection

Alek A. Petty[1, 2], Nicole Keeney[1, 2], Alex Cabaj[3], Paul Kushner[3], Marco Bagnardi[1, 4]
[1] Cryospheric Sciences Laboratory, NASA Goddard Space Flight Center, Greenbelt, MD, USA.
[2] Earth System Science Interdisciplinary Center, University of Maryland, College Park, MD, USA.
[3] University of Toronto, Toronto, Canada.
[4]ADNET Systems Inc., Bethesda, MD, USA.

Correspondence to: Alek A. Petty (alek.a.petty@nasa.gov)

Abstract

Reliable basin-scale estimates of sea ice thickness are urgently needed to improve our understanding of recent changes and future projections of polar climate. Data collected by NASA's ICESat-2 mission have provided new, high-resolution, estimates of sea ice freeboard across both hemispheres since data collection started in October 2018. Here we provide an impact assessment of upgrades to both the ICESat-2 freeboard data (ATL10) and NASA Eulerian Snow On Sea Ice Model (NESOSIM) snow loading on estimates of winter Arctic sea ice thickness. Misclassified leads were removed from the freeboard algorithm in the third release (rel003) of ICESat-2 freeboard data, which increased freeboards in January and April 2019, and increased the fraction of low freeboards in November 2018, compared to rel002. These changes improved comparisons of sea ice thickness (lower mean biases and standard deviations, higher correlations) with monthly gridded thickness estimates produced from ESA's CryoSat-2 (using the same input snow and ice density assumptions). Later releases (rel004 and rel005) of ICESat-2 ATL10 freeboards result in less significant changes in the freeboard distributions and thus thickness. The latest version of NESOSIM (version 1.1), forced by CloudSat-scaled ERA5 snowfall, has been re-calibrated using snow depth estimates obtained by NASA's Operation IceBridge airborne mission. The upgrade from NESOSIM v1.0 to v1.1 results in only small changes in snow depth which have a less significant impact on thickness compared to the rel002 to rel003 freeboard changes. Finally, we present our updated monthly gridded winter Arctic sea ice thickness dataset and highlight key changes over the past three winter seasons of data collection (November 2018 - April 2021). Strong differences in winter Arctic thickness across the three winters are observed, including a 50 cm decline in multi-year ice thickness. Mean first-year ice thicknesses across the three winters were negligible. Interannual changes in snow depth provide significant impacts on our thickness results on regional and seasonal scales. Our analysis of recent winter Arctic sea ice thickness variability is provided online in a Jupyter Book format to increase transparency and user engagement with our derived monthly gridded winter Arctic thickness dataset.

1 Introduction

NASA's Ice, Cloud, and Land Elevation Satellite-2 (ICESat-2) is providing significant advances in our ability to monitor Earth's fast-changing sea ice cover. The Advanced Topographic Laser Altimeter System (ATLAS) onboard ICESat-2 measures surface elevation at high resolution (individual laser footprints of ~11 m, Magruder et al., 2020) and high precision (< 2 cm over sea ice flat surfaces, Kwok et al., 2019a), with dense along-track sampling (70 cm along-track from the 10 kHz pulse repetition rate, Neumann et al., 2019). ATLAS was designed in part to obtain accurate and routine estimates of sea ice freeboard, the vertical extension of sea ice above local sea level, across the polar oceans (Markus et al., 2017). Sea ice freeboard can typically range from millimeters to tens of centimeters depending on the region or season profiled. ICESat-2 benefits from extensive polar coverage (profiling up to 88 degrees N/S, monthly sub-cycle) and has collected year-round data with minimal downtime since production started in October 2018. ICESat-2 sea ice height and freeboard data are provided in the official ATL07 (Kwok et al., 2021a) and ATL10 (Kwok et al., 2021b) products respectively. The first winter season of ICESat-2 Arctic Ocean sea ice freeboards (ATL10) was presented in Kwok et al., (2019b), highlighting the regional and seasonal freeboard distributions obtained by ICESat-2.

Validation of the ATL07 and ATL10 products is on-going. ATL07 sea ice heights showed very strong agreement (0 cm mean differences, correlation coefficients of 0.97 to 0.98) with coincident airborne data collected by NASA's Operation IceBridge north of Greenland and the Canadian Archipelago in spring 2019 (Kwok et al., 2019a). The freeboard agreement was more modest (mean differences of 0 to 4 cm), although the comparisons were hindered by the lack of available leads to reliably determine a local sea surface in either product. Additional analysis of the ATL07/10 surface classification scheme using imagery collected by the Copernicus Sentinel-2 mission, provided evidence of high skill in lead classification (Petty et al., 2021), a key part of the freeboard determination procedure. However, both the spring 2019 OIB Arctic campaign comparisons (Kwok et al., 2021d) and Sentinel-2 imagery assessments (Petty et al., 2021) highlighted errors in the 'dark lead' classification in ATL07/10. Briefly, it was hypothesized that low/optically thin clouds in these regions attenuate the photon rate around these segments due to increased atmospheric scattering, tricking the empirical threshold-based classification algorithm into characterizing height segments over sea ice as dark leads. High photon rate specular leads are now the only lead types used to derive sea surface and thus freeboard in the Release 003 and subsequent sea ice products (Release 005 at the time of writing) while a possible filter for the dark-lead segments is being developed and tested. The impact of this change was an increase in freeboard in ATL10 of 0 to 3 cm depending on the season/region analyzed, as well as a decrease in coverage due to the reduction in sea surface tie-points (Kwok et al., 2021d).

Measurements of sea ice freeboard are typically collected to estimate sea ice thickness, see schematic in Figure 1. This is conventionally achieved by combining freeboard measurements with ancillary estimates of snow loading (snow depth and density), sea ice density and an assumption of hydrostatic equilibrium (e.g. Giles et al., 2007; Kwok and Cunningham, 2008; Laxon et al., 2013; Kwok, 2018). Sea ice thickness was estimated from Release 002 ATL10 freeboards using external snow loading estimates from the NASA Eulerian Snow on Sea Ice Model (NESOSIM) v1.0 and modified versions of the

Warren et al. (1999) snow climatology (Petty et al., 2020, P2020). The Feb/March 2019 ICESat-2 thicknesses were ~10 cm thinner than Feb/Mar 2008 ICESat thickness estimates, alluding to a possible decline in end-of-winter Arctic sea ice thickness over this 11-year period. However, the P2020 thickness estimates were also significantly thinner than those produced using radar freeboard measurements from ESA's CryoSat-2 using the same input assumptions (tens of cm biases depending on the month and product analysed). Significant biases still exist in satellite-derived estimates of sea ice thickness, even those based on the same satellite sensor, e.g. radar altimetry data from ESA's CryoSat-2 mission (Sallila et al., 2019; Petty et al., 2020) which have limited their utility to-date, e.g. for constraining or calibrating polar climate projections (e.g. SIMIP Community, 2020).

The thickness results presented in P2020 used NESOSIM v1.0 snow loading forced by the European Centre for Medium-Range Weather Forecasts (ECMWF) ERA-Interim (ERA-I) snowfall (Dee et al., 2011). However, ERA-I production ended in August 2019 and was superseded by ERA5 (Hersbach et al., 2020). While ERA5 total precipitation is similar to ERA-I over the Arctic Ocean (Wang et al., 2019; Barrett et al., 2020), ERA5 produces relatively more snowfall and thus less rainfall compared to ERA-I, especially in the Atlantic sector of the Arctic (Wang et al., 2019). Additional developments and calibration of NESOSIM have been carried out to upgrade NESOSIM (v1.0 to v1.1) and extend the derived ice thickness product beyond the first winter season (2018/2019) presented in P2020 which we present here.

The significant changes in ATL10 freeboards and the availability of updated NESOSIM snow loading warrants an updated winter Arctic sea ice thickness assessment. ATL10 and NESOSIM v1.1 output are now also available from fall 2018 through to spring 2021, providing three winter seasons of data to assess. The main objectives of this paper are to: (i) highlight upgrades to the ICESat-2 ATL10 freeboard product and NESOSIM v1.1 snow loading and assess their impact on winter Arctic sea ice thickness; (ii) carry out updated comparisons against CryoSat-2 derived thickness estimates; and (iii) assess monthly gridded thickness data from the past three winter seasons across the entire Arctic Ocean. The monthly gridded thickness analysis is also available online in a Jupyter Book format (https://nicolekeeney.com/icesat2-book) to increase transparency and user engagement in our analysis of these data.

2 Data and Methods

2.1 ICESat-2 ATL10 freeboards

We use the ICESat-2 ATL10 sea ice freeboard product (currently at Release 005, rel005), which is disseminated through the National Snow and Ice Data Center (NSIDC) (Kwok et al., 2021a). ATL10 is the end result of a series of algorithms that convert the primary geolocated photon product (ATL03, Neumann et al., 2019), to sea ice height and type (ATL07, Kwok et al., 2021a), and then sea surface height and freeboard (ATL10, Kwok et al., 2021b). Briefly, the ATL07 algorithm subtracts a mean sea surface and time-varying ocean tide and inverted barometer corrections from ATL03, then aggregates and windows 150 photons around this corrected surface along each beam independently. ATL07 then extracts a best-guess Gaussian height distribution convolved with the expected system response to the photon height histogram to determine a

single 'segment' height and various metrics summarizing the goodness of fit and radiometry (e.g., photon rate) of each segment. This photon aggregation results in data with variable segment lengths of, on average, ~15 m for the strong beams and ~60 m for the weak beams (Kwok et al., 2019b). The spatial resolution of the individual segments can be estimated by adding the individual laser footprint size of ~11 m (Magruder et al., 2020) to the segment length, i.e., a mean of ~25 m for the strong beams and 70 m for the weak beams. An empirically based decision-tree algorithm is used to discriminate the height segments as either sea ice or sea surface/lead (Kwok et al., 2016). More details of the surface classification scheme are available in Kwok et al., (2021d) and Petty et al., (2021), while the complete processing methodology is available in the Algorithm Theoretical Basis Document (ATBD) for sea ice products (Kwok et al., 2021c).

ATL10 converts adjacent sea surface segments into lead groups to reduce noise in the lead height estimate and then averages these into 10 km along-track sea surface reference height estimates along each beam. Sea ice freeboard is calculated as the difference between the individual ice height segments and the local sea surface height, independently for each beam. The ICESat-2 beams are arranged in 'strong' and 'weak' beam pairs with each beam pair separated by ~3.3 kilometers in the across-track direction and the strong/weak beams separated by ~90 m across-track and ~2.5 km along-track. The weak beams are around 4 times lower energy (lower photon rate) than the strong beams. In this study we utilize only the strong beams to ensure the highest possible data quality.

2.1.1. ATL10 upgrades

The ICESat-2 sea ice products are continuously being updated as new assessments on the data are undertaken. All ICESat-2 products currently follow the same nominal release schedule (~6-12 months), so release updates are not necessarily based on the significance of the changes or improvements made to the given product. All new release data are processed and released from the start of the mission (October 14th, 2018) onwards, until the production of a new release begins. The sea ice thickness results presented in P2020 utilized rel002 ATL10 data, and differences with thickness estimates produced using rel001 ATL10 were noted to be negligible. As discussed earlier, in rel003 ATL10 and subsequent releases, dark leads have been removed as possible sea surface height segments, since false positive classifications were found in the presence of clouds, resulting in an increase in basin averaged freeboards of up to 3 cm and some loss in coverage, especially within the more consolidated central Arctic ice pack (Kwok et al., 2021d). This is arguably the biggest change in the ICESat-2 sea ice products to-date. The rel003 ATL10 data also included a relaxing of the height/freeboard quality flag (from 3 to 4), which means height segments with a poorer fit, generally segments from ridges with a more variable and complex height profile, are now included to increase retrieval counts over ridged ice regimes.

In rel004, most of the updates involved changes related to the treatment of the solid earth tides - a transition of ATL07 into a tide-free system to be consistent with ATL03. This caused a significant change in the magnitude of the heights reported in ATL07 and ATL10, but as freeboard is a relative measurement, this was not expected to impact the reported freeboards. In rel005 ATL10, the only changes relevant to freeboard determination include improved calculation of the 10 km reference surface location to the centre of each section (effectively a bug fix). The rel005 data now also includes data

from previously held granules where known satellite calibration scans were occurring somewhere along the granule. New automated pointing angle and calibration scan filters were introduced in rel005 to ensure only data within each granule experiencing degraded performance are filtered out, instead of withholding entire data granules. Most other developments in rel003 to rel005 ATL10 can be categorized as minor bug fixes and are listed in the ATBD change log, made available since rel004. New releases of ATL07 and ATL10 also reflect upgrades to the underlying ATL03 processing, such as improvements in geolocation.

In Figure 2we provide an assessment of the coverage change from rel002 to rel005 by counting the number of 10 km sea surface reference tie points available across the 4 releases from all data collected by the strong beams between November 2018 and April 2019. The analysis provides further evidence of the decline in coverage between rel002 and rel003. The rel003 to rel005 coverage differences are sporadic and linked mainly to the inclusion of calibration scan data granules. Calibration scans occur mainly over lower latitudes but can occasionally extend over the Arctic ice pack – data during these scans are generally considered degraded i.e., heights with sub-nominal geolocation quality. Automated calibration scan filtering was introduced in rel005 to exclude these data more reliably and ensure only the highest quality height returns are utilized. In Figure S1 we provide a beam coverage assessment over the same time period using rel005 data only, highlighting the consistently higher coverage provided by the strong beams compared to the weak beams across this first winter of data collection). The middle beam pair is notable for the higher reference counts compared to other strong and weak beams .

2.2 NESOSIM

We use snow depth and density estimates from the NASA Eulerian Snow On Sea Ice Model (NESOSIM) (Petty et al., 2018a, P2018) which is publicly available on GitHub (https://github.com/akpetty/NESOSIM). NESOSIM was developed primarily in preparation for the launch of ICESat-2, to enable timely production of snow depth and density estimates for sea-ice thickness retrievals using a simple snow accumulation model framework. NESOSIM includes two vertical snow layers and several simple parameterizations (accumulation, wind packing, advection–divergence, blowing snow loss) to represent the expected primary sources and sinks of snow on Arctic sea ice during the accumulation season. Summer melt processes are currently neglected, so the model is typically run between September and the end of April. NESOSIM v1.0 was first presented in P2018 and the output using this v1.0 framework was used in P2020 to produce snow loading needed to convert ATL10 freeboards (rel002) to sea ice thickness from October 2018 to April 2019. The NESOSIM v1.0 output used in P2020 was forced with snowfall, winds and near-surface air temperature (to scale the initial snow conditions) from ERA-I (Dee et al., 2011), sea ice concentrations from the NASA Climate Data Record (CDR) version 3 (Meier et al., 2017), and ice drifts from the European Organization for the Exploitation of Meteorological Satellites (EUMETSAT) Ocean and Sea Ice Satellite Application Facility (OSI SAF) (Lavergne et al., 2010) which were all regridded to a 100 km x 100 km Arctic Ocean domain.

2.2.1. NESOSIM upgrades

Here we describe recent upgrades made to NESOSIM which has been tagged as a new version 1.1 (v1.1) code release (https://github.com/akpetty/NESOSIM/releases/tag/v1.1, archived at https://doi.org/10.5281/zenodo.4448356). Key updates in NESOSIM v1.1 include: CloudSat snowfall scaling (Cabaj et al., 2020, and described more below), a new blowing snow atmosphere loss term, an extended Arctic domain to cover the full extent of the Arctic peripheral seas, an improved smoothing filter to reduce noise in the dynamic snow budget terms, an upgrade to Python 3, and various minor bug fixes. Much of the NESOSIM v1.1 development was motivated by the need to recalibrate NESOSIM using ERA5 forcings (Hersbach et al., 2020), now that ERA5 has succeeded ERA-I following the end of ERA-I data production in August 2019 and given reports of increased ERA5 snowfall compared to ERA-Interim (Wang et al., 2019; Cabaj et al., 2020). ERA5 is thought to offer improvements over ERA-I related to improved cloud representation, an updated assimilation scheme and higher spatial resolution (Hersbach et al., 2020). Regardless, whether ERA5 exhibits a high snowfall bias over the Arctic or ERA-I a low bias is still uncertain and likely regionally dependant. Cabaj et al., (2020) used snowfall estimates from CloudSat to calibrate several reanalyses snowfall estimates, including ERA5, within the NESOSIM framework – reducing the spread in snowfall from the chosen reanalyses, although not significantly changing the magnitude of the ERA5 snowfall in the North Atlantic region, where winter snowfall rates are highest overall. On average, ERA5 reports more snowfall over the Arctic basin than what is observed by CloudSat measurements, so the scaling tends to slightly decrease the overall magnitude of the snowfall and the resulting snow depth in NESOSIM (Cabaj et al. 2020). The CloudSat-reanalysis scaling coefficients are now included in the NESOSIM v1.1 code repository.

The other significant code development was the introduction of a new blowing snow loss term. The simple parameterization of blowing snow lost to leads/open water in NESOSIM v1.0 (Eq. 10 in P2018) has been challenged due to uncertainties around how much snow might be lost to open water under windy conditions, rather than sublimated, i.e. lost to the atmosphere, or transported either within or to adjacent grid-cells (Liston et al., 2020). Motivated by this, we introduced an additional blowing snow atmosphere loss term, which is a similar function of wind speed and snow in the top 'new' snow layer to the loss-to-open water term, but not also a function of sea ice concentration:

$$\Delta h_s^{bs\_a} = \gamma T_d U h_s \quad \text{for } U > \omega \quad [1]$$

where h_s is the snow depth in the top 'new' snow layer, U is the wind speed, T_d is the number of seconds in the daily time-step, ω is the wind action threshold, and γ is a new blowing snow atmosphere loss coefficient. This parameterization, which provides a simple mechanism for increasing snow loss under given atmospheric conditions independent of sea ice conditions, requires calibration of an additional free parameter, γ. As discussed in the original NESOSIM study (Petty et al., 2018), these snow loss terms are crude representations of complex physical processes that we introduce primarily to remove snow and improve correspondence with the limited observations we have for calibration purposes.

Additionally, NESOSIM v1.1 was forced with daily sea ice concentrations from the NASA Climate Data Record (CDR) version 3 (Meier et al., 2017), daily ice drifts from both the NSIDC Polar Pathfinder version 4 dataset (Tschudi et al., 2019) from 1980 to April 2019 and daily drifts from the European Organization for the Exploitation of Meteorological Satellites (EUMETSAT) Ocean and Sea Ice Satellite Application Facility (OSI SAF) global low resolution ice drift dataset (Lavergne et al., 2010) from September 2019 to April 2021 due to contrasting data availability. As noted in P2018, the impact on snow depth from ice drift forcing is generally second order to snowfall, although this can have first-order impacts at more regional scales. All forcings were regridded to our updated 100 km x 100 km North Polar Stereographic (EPSG: 3413, https://epsg.io/3413) Arctic Ocean model domain.

We recalibrated NESOSIM v1.1 considering the new forcings and model changes described above, by targeting estimates of spring Arctic snow depths derived from Snow Radar data collected during NASA's Operation IceBridge as used in P2018: the snow radar layer detection (SRLD) product (Koenig et al., 2016), the NASA Goddard Space Flight Center (GSFC) empirical threshold based product (Kurtz et al., 2013) and the Jet Propulsion Laboratory (JPL) product (Kwok et al., 2017). Our approach differs from the calibration approach used in P2018, which calibrated NESOSIM v1.0 against Soviet Station drifting station data collected in the 1980s (Warren et al., 1999) then assessed these results against OIB-derived snow depths. Here we choose instead to recalibrate NESOSIM v.1.1 against the spring OIB snow depth data from 2010 to 2015 to provide a more reliable snow depth representation focussed on our contemporary period of interest. We retain, however, the density values for the new 'top' and old 'bottom' layer snow (Table 1) which were derived from the Soviet Station calibration effort.

As noted in P2018 and presented in (Kwok et al., 2017), there is a large spread between the available OIB snow depth products due to various challenges in interpreting Snow Radar data. To account for this large inter-product uncertainty, we develop a 'consensus' gridded OIB spring snow depth product. We take all raw (~7 m along-track resolution) snow depth measurements from the three snow depth retrieval algorithms for a given day, bin them to the 100 km x 100 km NESOSIM v1.1 Arctic Ocean model domain using a simple binning procedure (average of all snow depths in the given grid-cell in each day), then take the median snow depth value at each daily grid-cell across the three OIB products. Quick-Look (QL) snow depths are available for the more recent years (2012 to 2019), using the GSFC waveform fitting approach (https://nsidc.org/data/NSIDC-0708/versions/1). However, it was noted in Kwok et al., (2017) that these estimates tend to exhibit a low bias compared to the other OIB products. A low bias in the GSFC QL product was also shown based on in-situ measurements collected in March 2014 (King et al., 2015). These biases were confirmed in our own analysis comparing our consensus OIB snow depths with the GSFC QL product (2013-2015), showing mean biases of ~6 cm (QL thinner than our consensus product, see Supplementary Figure S2), motivating us to exclude these from our model calibration efforts here.

We heuristically calibrated NESOSIM v1.1 using the daily OIB consensus gridded snow depths with the aim of removing the mean bias relative to OIB when using the default NESOSIM v1.0 parameter settings (Figure 3a). Current work is exploring more automated calibration approaches (Cabaj et al., 2021), but here we were able to find a solution that reduced the mean bias to 0 cm by halving the blowing snow open water coefficient, extending the model initialization date to

September 1 instead of August 15 and tuning the new atmosphere snow loss coefficient, γ, as shown in Figure 3b. In the absence of contemporary ground-truth data, we view the initial conditions (either their distribution or the representative start date) as another tuning parameter, constrained mainly by limited evidence in the literature. For example, the Warren et al., (1999) climatology (W99) shows a mean snow depth of 3 cm in August including depths of up to 8 cm near the Greenland/Canadian Arctic coastline based on the quadratic fit to observations. However, output from SnowModel-LG presented in Stroeve et al., (2020) shows zero snow depths in August in the earlier (1985/1986) and later (2015/2016) time periods of that time-series. As NESOSIM includes no snow melt terms, we prefer instead to initialize later in the year (Sep 1st) and prescribe an expected end of August mean snow depth based on our original temperature scaled W99 August climatology. NESOSIM v1.1 was run from 1980 to 2021 and is expected to be updated in future years to enable continued thickness processing from ICESat-2.

The output from this v1.1 model framework from 1980-2021 has been archived on Zenodo (https://doi.org/10.5281/zenodo.5164314). The NESOSIM v1.0 output from P2018 was originally released from 2000 to 2015 only but was extended for the 2018/2019 winter to produce snow depths used in the initial P2020 ICESat-2 sea ice thickness processing.

Figure 4 shows a time-series comparison of the October and April mean snow depths from NESOSIM v1.0 and v1.1 within an Inner Arctic Ocean domain (Central Arctic, Beaufort Sea, Chukchi Sea, Laptev Sea, Kara Sea). Our Inner Arctic Ocean domain was generated using a new National Snow and Ice Data Center (NSIDC) regional mask of the Arctic Ocean courtesy W. Meier and S. Stewart, shown in Figure 5. NESOSIM v1.1 shows good agreement with v1.0 in terms of the October and April mean snow depth and patterns of interannual variability. Differences between the two releases are <5 cm and often near zero. The longer record of NESOSIM v1.1 output is strongly suggestive of a long-term declining trend in snow depth and near-record low snow depths in recent years, i.e., the ICESat-2 period 2018-2021. To place the ICESat-2 period results in broader context, Figure 4 shows the monthly mean NESOSIM v1.1 snow depth distributions as violin plots, with the recent ICESat-2 years overlaid. In the initial accumulation months of September/October, recent years show similar or deeper than average snow, while the middle/end-of-winter months, November to April, show clearly thinner than average snow in the recent ICESat-2 years. The 2019-2020 and 2020-2021 snow depths especially are at or near record low values across most of these months, with 2020-2021 April at the record low, while 2019-2020 and 2018-2019 are instead near to the mean. Capturing this interannual variability was the key motivating factor behind the development of NESOSIM and its use in the thickness processing which we discuss more in the following sections.

Finally, a Quick Look (~2-3-day latency) ATL10 sea ice freeboard product was recently made available on the NSIDC (https://nsidc.org/data/ATL10QL). Producing near-real time NESOSIM output to derive near-real time thickness estimates is challenging due to the reliance on various forcing datasets from different international groups released at different latencies. A common approach taken by the community, e.g., the CryoSat-2 products highlighted in Section 2.4, is to utilize a modified Warren climatology (Warren et al., 1999), which we refer to herein as mW99, where the quadratic fit to snow observations collected by Soviet drifting stations is halved over first-year ice to crudely represent the transition in snow

expected from our more recent younger Arctic ice pack. To provide a simple alternative to mW99 for near-real time snow and ICESat-2 thickness assessments, we also calculate a modern-era representation of the NESOSIM v1.1 output (NESOSIM v1.1_2010-2020ave) by simply taking the mean NESOSIM snow depth and density value for each day of the year in each grid-cell averaged across the period September 1, 2010, to April 30, 2020. The NESOSIM v1.1_2010-2020ave results and mW99 averaged within the Inner Arctic Ocean domain (Figure 5) are also highlighted in Figure 4, while maps of the spatial differences between NESOSIM v1.1_2010-2020ave and mW99 in October and April are provided in the Supplementary Information (Figure S3). Briefly, at the start of winter (October), NESOSIM v1.1_2010-2020ave shows thinner snow depths in the Central Arctic but thicker snow depths in the Kara Sea, a region where mW99 is highly unreliable due to the lack of original input data. NESOSIM v1.1_2010-2020ave shows thinner snow depths in the Central Arctic at the start of winter (October) but thicker snow depths in the Kara Sea, a region where mW99 is questionable due to the lack of input snow depths. In April, NESOSIM v1.1_2010-2020ave shows thinner snow depths in the multi-year ice region of the Central Arctic, but thicker snow in the first-eyar ice regimes, especially in the Kara Sea as in October.

2.3 ICESat-2 sea ice thickness data upgrades

We use the same approach as in P2020 to generate estimates of winter Arctic sea ice thickness and an associated uncertainty estimate. Briefly, thickness is calculated assuming hydrostatic equilibrium and input estimates of sea ice density, snow depth and snow density. The coarse resolution (~100 km) snow depth input estimate, primarily from NESOSIM, is redistributed to the high-resolution (~30 m) ATL10 freeboards using a piecewise functional fit obtained from snow depth and freeboard data collected by NASA's Operation IceBridge mission (Kurtz et al., 2009; Petty et al., 2020). Uncertainties are calculated by propagating errors through the hydrostatic equilibrium equation with contributions from random errors (estimates based on previous studies) and systematic errors (estimates based on the spread in applied input assumptions). Small differences in our thickness processing to that presented in P2020 include a bilinear interpolation scheme instead of nearest neighbour to assign NESOSIM data to the ATL10 freeboard segments. Nearest neighbour interpolation was originally used to reduce processing time but introduces unphysical step changes. We also fixed some minor bugs in the freeboard uncertainty calculation and have incorporated the new NSIDC regional mask of the Arctic Ocean (Figure 5). As in P2020 we use daily estimates of ice type from the European Organization for the Exploitation of Meteorological Satellites (EUMETSAT) Ocean and Sea Ice Satellite Application Facility (OSI SAF, www.osi-saf.org) (Breivik et al., 2012) to classify each segment as either first-year ice (FYI) or multiyear ice (MYI). Ice type information is needed in-part to derive the modified Warren snow depth estimates (see Section 2.2.2. in P2020), so our approach is to assume all ice is MYI unless the OSI SAF product explicitly characterizes the segment as FYI. Thus, in September when OSI SAF does not provide any ice type estimate due to added uncertainties in the end-of-summer retrievals, we assume all our ATL10, and derived thickness data are MYI. The along-track thickness data, both raw segment-scale data and 10 km means, have been made available through the NSIDC (IS2SITDAT4 Version 1, https://nsidc.org/data/is2sitdat4/, Petty et al., 2022). We plan to update this dataset each year as new winter Arctic ATL10 data are generated and released.

In producing the monthly gridded dataset, we use all three strong beams to increase coverage and lower expected uncertainties, compared to the single strong beam used in P2020. The use of all three strong beams was also motivated by the reduction in data coverage in rel003 and onwards ATL10 data processing (described in Section 2.1.1 and noted in Figure 2). Our gridding approach is slightly different from the official gridded ICESat-2 freeboard product (ATL20, https://nsidc.org/data/ATL20) as we bin all data within a given month for each grid-cell, as opposed to producing daily gridded composites then monthly gridded composites from the daily gridded data. Our monthly gridded data includes ancillary data variables representative of the mean day of the month for each grid-cell calculated as the mean date of the input ATL10 data, and the number of ATL10 freeboard segments used in the monthly grid-cells to enable sampling bias assessments. The monthly gridded data also includes monthly NOAA/NSIDC Version 4 Climate Data Record (CDR) sea ice concentrations (Meier et al., 2021), the new NSIDC regional mask of the Arctic Ocean (courtesy W. Meier and S. Stewart, NSIDC) and the OSI SAF ice type mask (sub-sampled by ICESat-2 then gridded monthly). The data are projected on to the NSIDC North Polar stereographic grid (EPSG: 3411, https://epsg.io/3411) and binned onto a 25 km x 25 km grid.

The initial version of our monthly gridded thickness dataset as described in P2020 was made available through the NSIDC (IS2SITMOGR4 Version 1, https://nsidc.org/data/IS2SITMOGR4). Our updated dataset presented in this study using rel005 ATL10 data, updated NSIDC Arctic region mask and CDR sea ice concentrations have been made available as a new Version 2 (v2) release of the IS2SITMOGR4 dataset (Petty et al., 2022b). We expect to update this each year along with the along-track product (IS2SITDAT4) as new winter Arctic ATL10 data are made available. We also include in this Version 2 IS2SITMOGR4 dataset smoothed and interpolated variables of freeboard, snow depth and thickness in an initial attempt to fill in the pole hole and mitigate the spatial sampling biases. These preliminary variables are not used in the subsequent analysis presented here but their derivation are described and made available to interested users in the online Jupyter Book discussed below. We expect that future work will explore more sophisticated interpolation procedures and blending with other thickness datasets, which we discuss more in the summary section.

2.4 CryoSat-2 sea ice thickness estimates

Following P2020 we compare our winter Arctic sea ice thickness estimates with those generated from the European Space Agency (ESA) CryoSat-2 mission from four different groups: NASA's Goddard Space Flight Center (GSFC, Kurtz and Harbeck, 2017), the Jet Propulsion Laboratory (JPL, Kwok and Cunningham, 2015), the Center for Polar Observation and Modelling (CPOM, Laxon et al., 2013; Tilling et al., 2018) and the Alfred Wegener Institute (AWI, Hendricks and Ricker, 2016). As the different products make different assumptions regarding snow loading and sea ice, for these comparisons we use the same snow loading assumptions in our ICESat-2 thickness processing to generate direct thickness comparisons (instead of the NESOSIM based thickness estimates). As in P2020 we re-grid the monthly gridded CS-2 estimates to the NSIDC 25 km x 25 km North Polar Stereographic grid using a simple nearest neighbor interpolation scheme and compare these with our gridded ICESat-2 sea ice thickness estimates that have been produced using the same snow loading and ice

density assumptions as the given CS-2 product, as summarized in Table 2 in P2020. Note that in the CryoSat-2 comparisons we produce monthly gridded data using strong beam #1 only to be consistent with the results shown in P2020.

Modified versions of the Warren snow depth climatology (mW99, Warren et al., 1999) were used by all four of these CryoSat-2 thickness products, however it is worth noting that most of these groups are actively working on incorporating more sophisticated snow loading models. P2020 noted strong differences between NESOSIM v1.0 and mW99 (mW99, snow depths halved over first-year ice, see Supplementary Figures S2 to S4 in P2020). Generally, snow depths are similar over the thicker multiyear ice, but mW99 is thinner later in the year, due primarily to the reduced snow over first-year ice. Figure 4 shows the mean Inner Arctic Ocean snow depth from mW99 (snow depths halved using observed OSI SAF ice types from 2010 to 2019), showing similar values to NESOSIM in October but thinner mW99 snow in April. Again, we use the same snow loading when producing comparison ICESat-2 thickness estimates, but it is worth noting that these thickness estimates will be different to our NESOSIM-derived thickness product due to these differences in snow.

2.5 PIOMAS sea ice thickness estimates

We additionally compare our gridded winter Arctic sea ice thickness estimates with those generated from the Pan-Arctic Ice-Ocean Modeling and Assimilation System (PIOMAS, v2.1; Zhang & Rothrock, 2003). PIOMAS is an ice-ocean model that generates estimates of sea ice thickness, constrained predominantly by the assimilation of sea ice concentration and sea surface temperature. PIOMAS data is commonly used in the sea ice community for assessments of Arctic sea ice thickness variability at regional and basin-scales (Tilling et al., 2015; Labe et al., 2018; Petty et al., 2018b; Schweiger et al., 2021; Moore et al., 2018). PIOMAS ice thicknesses estimates have been shown to exhibit differences on the order of tens of centimeters compared to satellite-derived estimates, although this depends strongly on the season and region analyzed (Schweiger et al., 2011; Zygmuntowska et al., 2014; Petty et al., 2018b).

2.6 ERA5

To assess winter Arctic atmospheric conditions, we utilize near-surface (2 m) air temperature and downwelling longwave radiation estimates from the ERA5 reanalysis (Hersbach et al., 2020). A warm bias of X DEGREES in 2 m air temperatures over Arctic sea ice has been noted in comparisons with drifting buoys (Wang et al., 2019; Yu et al., 2021) which has been linked to poor representation of sea ice thickness and snow cover in reanalyses (CITE). We utilize these data with caution and focus primarily on basin-scale, monthly averaged assessments.

3 Results

3.1 ATL10 freeboards, NESOSIM snow loading and sea ice thickness distributions

In Figure 6 we show probability distributions of winter Arctic sea ice freeboard calculated using rel002 (as used in P2020) through to rel005 ATL10 data. We show distributions from November 2018, January 2019, and April 2019 to assess

differences during different regimes of winter Arctic sea ice (early, middle and late winter) for the first season of data collection. The distributions use data collected by strong beam #1 only within an Inner Arctic Ocean domain (Central Arctic, Beaufort Sea, Chukchi Sea, Laptev Sea, Kara Sea). Note that in these distributions we show only positive values of freeboard and later snow depth and thickness, while in the raw along-track IS2SITDAT4 dataset zero freeboards, typically from open water lead segments, are included also.

Figure 6 shows that the only notable change in freeboard distribution occurs between rel002 and rel003 - a freeboard decrease of 1.2 cm in November 2018 (26.2 cm to 25.0 cm), a 1.9 cm increase in January 2019 (27.7 cm to 29.6 cm) and a 3.4 cm increase in April 2019 (35.9 cm to 39.3 cm). In contrast, the rel003 to rel005 freeboard distribution differences across these three months are small or negligible (<0.4 cm). Rel005 generally shows the highest freeboards from the four releases. As discussed earlier, this was largely expected due to the major algorithm change in rel003 (Kwok et al., 2021d) and the lack of major algorithm changes related to freeboard derivation in rel004 and rel005. The 1.2 cm mean freeboard reduction in November 2018 is due to a more significant primary freeboard peak and a less significant secondary peak in the rel003 to rel005 freeboard distributions, while January 2019 and April 2019 distributions exhibit a clear increase in the unimodal freeboard in rel003 onwards. Kwok et al., (2021d) analysed gridded freeboard distributions in January 2019, June 2019, October 2019 and found 3 cm, 1 cm and 2 cm increases respectively between rel002 and rel003, in-line with the differences observed here. As discussed in Section 2.1.1 and demonstrated in Figure 2, the different releases also include changes in coverage, especially between rel002 and rel003, which may influence these differences along with changes in the freeboard determination algorithm.

Figure 6 (right column) also shows an analysis of the inter-beam differences across the three strong beams for the same time periods and Inner Arctic Ocean region for rel005 data only. The inter-beam differences are small (<1 cm), similar to the rel003-rel005 differences. Each strong beam is separated by ~3 km across track, so more significant differences are expected at local scales, however an in-depth analysis of spatial length-scales is beyond the scope of this study. We instead note that at basin/monthly scales, the beams provide similar freeboard distributions despite the small differences in coverage (as discussed in Section 2.1.1 and highlighted in Figure S2), increasing our confidence in using all three beams to extend coverage across the Arctic.

Figure 7 shows the impact of three different NESOSIM frameworks (v1.0, v1.1 and v1.1_2010-2020ave) based on rel004 freeboards on the redistributed snow depths (these assessments were carried out during the period of rel004 availability). The piecewise redistribution of the coarse 100 km NESOSIM output to the high-resolution ATL10 data is summarized in Section 2.3 and presented in P2020. The difference in mean snow depth across the three months and NESOSIM frameworks is < 1.5 cm, with the biggest difference occurring in the November 2018, where the Nv1.1 redistributed snow depths are thicker than the Nv1.0 snow depths (17.0 cm compared to 15.5 cm) driven primarily by a small positive shift in the tail of the distribution. The January and April mean snow depths are similar across the NESOSIM frameworks, although slight differences in the distributions are observed, e.g., a thinner secondary snow depth peak in NESOSIM v1.1 compared to v1.0 (~22 cm compared to ~26 cm). The NESOSIM v1.1_2010-2020ave results are similar,

although noteworthy for the more distinct secondary snow depth peak (~28 - 29 cm) and thicker primary peak (~4-5 cm thicker) in the November 2018 and January 2019 distributions compared to the v1.0/v1.1 snow depths. All distributions capture the same general seasonal evolution (distributions and mean values) and show a similar unimodal snow depth distribution in April 2019.

Figure 7 (right column) shows the impact of the different NESOSIM frameworks on estimates of sea ice thickness. The difference in mean sea ice thickness across the three months and NESOSIM frameworks is greatest in November 2018: v1.1-derived thicknesses are 10 cm thinner than v1.0 while the v1.1_2010-2020ave-derived thicknesses show a higher primary peak but longer tail. The thickness differences across the three NESOSIM frameworks are 4 cm in January 2019 and 2 cm in April 2019. In general, the impact on thickness from the choice of NESOSIM framework, including the NESOSIM modern-era mean output, is less significant than the impact from rel002 to rel003 freeboard changes.

3.2 Comparisons with CryoSat-2

In Figure 8, we show the correlation coefficients, mean bias and standard deviation of differences between monthly gridded ice thickness from rel002 and rel003 ICESat-2 data and thickness estimates produced with ESAs CryoSat-2. In these thickness comparisons we generate monthly gridded thickness estimates using the same input assumptions, i.e., mW99 for snow loading (See Section 2.2.1 and Table 2 in P2020). As in P2020 we only use strong beam #1 and mask all data below 0.25 m and outside of an Inner Arctic Ocean domain in both datasets before producing these comparisons to focus more on the representation of consolidated pack ice between the two sensors, rather than the added complexities of thin and marginal ice.

In general, the agreement between ICESat-2 and CryoSat-2 using rel005 ATL10 freeboards is improved compared to those based on rel002 ATL10 freeboards in terms of the correlation coefficient, mean bias and standard deviation across most months and products. In November 2018 the correlation coefficient increases from 0.66 - 0.77 (rel002 ATL10) to 0.80 - 0.88 (rel005 ATL10), the mean bias reduces from 0.35 m – 0.65 m to 0.20 m – 0.55 m and the standard deviation reduces from 0.60 m - 0.79 m to 0.40 m - 58 m across the four product comparisons. In January 2019 the correlation coefficient increases from 0.55 - 0.65 (rel002 ATL10) to 0.60 - 0.72 (rel005 ATL10), the mean bias reduces from 0.35 m – 0.50 m to 0.05 m – 0.22 m and the standard deviation reduces from 0.58 m - 0.77 m to 0.50 m – 0.62 m. In April 2019 the correlation coefficient increases from 0.20 - 0.40 (rel002 ATL10) to 0.39 - 0.55 (rel005 ATL10), the mean bias reduces from 0.02 m – 0.35 m to -0.30 m – -0.05 m and the standard deviation reduces from 0.95 m – 1.07 m to 0.68 m – 0.80 m. The statistics from all months between November 2018 and April 2019 are shown in Figure 8. More work is needed to better reconcile these datasets and assess sources of bias (as discussed more in the summary) but these results represent an encouraging initial development in terms of the ICESat-2 sea ice freeboard and thickness product development.

3.3 Gridded Arctic sea ice thickness and comparisons over the last three winters.

In Figure 9 we show an example output of our updated monthly gridded ICESat-2 winter Arctic sea ice thickness product (IS2SITMOGR4 version 2, v2) for April 2021 using the latest default thickness processing configuration (rel005 ATL10 and NESOSIM v1.1 snow loading). Spatial coverage is high across all months (not shown) despite the concerns expressed in Kwok et al., (2021d) related to reduced lead/sea surface height segments and thus freeboard determination. This was partly mitigated by our use of 3 strong beams (coverage changes were discussed in Section 2.1.1). Despite our use of three strong beams, there are still large regions of missing data in our monthly gridded dataset, e.g., the missing data in the Laptev/East Siberian Sea shown in Figure 9 despite the monthly CDR ice concentrations showing concentrations greater than 50% in that same region. Data drop-out is often caused by the presence of clouds and the resultant atmospheric scattering impacts on ATLAS retrievals. Our interpolated/smoothed variables of freeboard, snow depth and thickness data (Figure 9i-j, not used in this study) do not substantially increase coverage in these regions, which was in-part by design to avoid over-extrapolation of our thickness estimates. In general, the monthly gridded data gaps are limited but should be considered when using these data to assess regional and basin-scale thickness variability.

Our following analysis of the monthly gridded ICESat-2 winter Arctic sea ice thickness data across the first three winters of data collection is a subset of the analysis presented in our online Jupyter Book (https://nicolekeeney.com/icesat2-book/sea_ice_characteristics.html). The Jupyter Book consists of a series of Jupyter Notebooks that provide all code and analysis output written in the Open-Source Python programming language for demonstrating and sharing our thickness analysis workflow. The development of the Jupyter Book was motivated by the desire for transparency and the broader goals of facilitating more open science, but also the desire to provide a simple mechanism for interested users to explore regions and time periods not shown here. For example, the Jupyter Book allows users to adapt the code interactively, either locally or using Binder, to select months and regions of interest to explore characteristics of this dataset beyond the core figures we show here.

In Figure 10 we show the seasonal evolution of winter freeboard, snow depth/density and sea ice thickness from our IS2SITMOGR4 v2 monthly gridded dataset. The results shown in Figure 10 are again restricted to our Inner Arctic Ocean domain using the included NSIDC Arctic region mask (Figure 5) to simplify interpretation and avoid regions of higher uncertainty within the more peripheral seas of the Arctic. The data within this domain in September and October is generally lower concentration (40-60% on average, Figure 10e), than the proceeding months (~90% in November and near 100% in December through April), so changes in early winter are still strongly influenced by the changing coverage of sea ice as the ice pack refreezes. Note that the concentration decline from September to October is due to changes in data coverage as regions with ice concentrations < 50% are not included in ATL10 and thus our thickness estimates. We therefore mainly focus on analysing November to April changes, the period in which we also have full monthly data available across all three winters.

Mean monthly Inner Arctic Ocean sea ice freeboard from ATL10 show a monotonic increase from 22 cm in November 2018 to 38 cm in April 2019. Mean monthly freeboards in November 2019 are similar to 2018, but consistently lower in subsequent months (lower by ~2-3 cm). Mean freeboards in November 2020 are significantly lower than the previous two winters (20 cm mean, so lower by ~2-3 cm), and are similar or lower than the 2019-2020 monthly means (lower by ~1-2 cm).

Mean monthly Inner Arctic Ocean snow depths from the redistributed NESOSIM v1.1 output monotonically increase from 14 cm in November 2018 to 24 cm in April 2019, increasing more rapidly between January and April than between November and January. Snow depths in the 2019-2020 winter show a similar seasonal evolution but with snow depths consistently ~ 2 cm thinner than the 2018-2019 monthly means. The 2020-2021 snow depths are similar to 2019-2020, showing thicker snow in January 2021 compared to January 2020 but thinner snow in April 2021 than April 2020 and 2019. The mean seasonal snow density evolution is similar across the three winters, with the 2020-2021 density lower in November than the previous winters but notably higher than the previous winters between February and April. Due to the crude nature of the NESOSIM density parameterization, we do not view this analysis as a reliable interannual snow density assessment but highlight this more to understand the density variability impact on our ice thickness estimates.

Our mean monthly estimates of Inner Arctic Ocean sea ice thickness show an increase from 1.20 m +/- 0.30 m in November 2018 to 2.0 m +/- 0.35 m in April 2019, with the monthly thickness increasing more rapidly between November and February than between February and April. The 2019-2020 monthly mean thickness evolution is similar to 2018-2019 winter, but with a lower April 2020 mean thickness of 1.90 m +/- 0.35 m compared to April 2019. The 2020-2021 mean thicknesses are significantly thinner in November through February compared to the previous two winters, ~0.9 m +/- 0.3 m in November 2020 to 1.90 m +/- 0.35 m in April 2021. Analyzing just these three winters, we observe significant differences in winter Inner Arctic Ocean thickness, with variability in the NESOSIM snow depth, and density to a lesser extent, modulating a significant component of the seasonal freeboard differences observed by ICESat-2. For example: thinner 2019-2020 snow compared to 2018-2019 mitigate the thinner freeboard and results in similar mean thickness across both winters; thinner April 2021 snow compared to 2020 and 2019 April snow mitigates the thinner freeboard and similarly results in a similar mean thickness. It is also worth noting that the fraction of multi-year ice is inversely related to the thickness rankings – i.e., the 2018-2019 winter shows the lowest mean fraction of multi-year ice in this three-year period, but also shows the highest freeboard, snow depths and thickness. Three years is not a long enough record to establish true relationships, but the results highlight the potential pitfalls of inferring thickness from ancillary quantities such as freeboard or multi-year ice fraction if one is interested in tracking interannual changes.

To assess the spatial distribution of the winter changes discussed above, Figure 11 shows maps of winter mean (November to April) freeboard, snow depth and thickness from IS2SITMOGR4 v2, while Figure 12 shows anomalies relative to the three-winter mean. The winter mean freeboard maps show positive anomalies in the 2018-2019 winter in the region directly north of Greenland and the Canadian Arctic Archipelago (CAA), the region of the Arctic where we generally expect to observe the thickest freeboard, snow depth and thickness. Some small negative freeboard anomalies are observed

in the Beaufort Sea and within Bering Strait. The 2018-2019 snow depth anomalies are relatively small and regionally variable while the 2018-2019 thickness anomalies are similar to the freeboard anomalies except for the additional weak negative anomalies that extend from the Beaufort Sea across the Central Arctic and into the Barents Sea. The 2019-2020 freeboard anomalies show instead weak regionally variable anomalies, including negative anomalies along the CAA coast. The 2019-2020 snow depth anomalies show similar spatial distributions to freeboard except for the positive Laptev Sea snow depth anomalies and stronger positive central Arctic snow depth anomalies. The impact on 2019-2020 thickness is weak negative anomalies in the eastern Arctic and some strong negative anomalies along (and within) the CAA coast and weak positive anomalies in the Central Arctic. Data within the CAA should be treated with caution as the lack of leads in these narrow channels often hinder freeboard/thickness retrievals. These are not included in the mean timeseries plots shown in Figure 10 partly for this reason. The 2020-2021 freeboard anomalies show a regional distribution almost opposite to 2018-2019, with strong negative anomalies in the Southern Central Arctic region north of Greenland/CAA and towards the Barents Sea, with weak positive anomalies in the Beaufort, Laptev, Bering Seas and Hudson Bay. The spatial distribution in the 2020-2021 snow depth anomaly is again variable and notable for the strong negative anomalies within the Barents Sea. The strong negative Barents Sea snow depth anomalies mitigate much of the negative freeboard anomalies observed by ICESat-2, meaning the impact on the 2020-2021 thickness is strong negative anomalies throughout much of the Central Arctic region and into the Chukchi Sea. The low freeboards within the Barents Sea region and the increased potential for surface flooding in this region (Granskog et al., 2017), a process which is not currently simulated by NESOSIM, means those results should also be treated with caution (this region is mostly excluded from our Inner Arctic Ocean domain, Figure 5). Monthly maps and anomalies of all IS2SITMOGR4 v2 variables have been generated and provided in the relevant Jupyter Book page (https://nicolekeeney.com/icesat2-book/sea_ice_characteristics).

In Figure 13 we show a comparison of these three winters of Inner Arctic Ocean sea ice thickness and associated uncertainties with thickness estimates derived from PIOMAS. As opposed to the CryoSat-2 comparisons, we focus here on basin-scale comparisons to assess the broad level of agreement when using both datasets for assessing the winter seasonal cycle and interannual thickness variability – arguably the primary use of PIOMAS data to-date. In general, both seasonal timeseries show good agreement, however PIOMAS is generally thicker than ICESat-2, especially by the end of winter in all three years of our analysis (20 to 40 cm thicker). These differences are within the spread of our ICESat-2 systematic uncertainty estimates, however. Spatial difference plots are generated and provided in the Jupyter Book (https://nicolekeeney.com/icesat2-book/pio_vs_is2) which highlight the stronger disagreement at regional scales, e.g., PIOMAS not simulating the thicker ice north of the Greenland and CAA coasts shown in our ICESat-2 data.

During the peer review of this paper, another studied was published utilizing joint ICESat-2 ATL10 and CryoSat-2 freeboard estimates to derive snow depth and thickness concurrently assuming that ICESat-2 measures total (ice plus snow) freeboard and CryoSat-2 can be used to infer ice freeboard (Kacimi and Kwok, 2022). Their results analyzed within a similar Inner Arctic Ocean region show encouraging agreement with the results presented here using independent snow loading assumptions: (i) snow depths increasing from ~10 - 12 cm in November to ~20-22 cm in April, ~2 cm thinner than our snow

depths but with a similar overall decline of ~3 cm over the three year period and (ii) thickness increasing from ~1.0 - 1.3 m in November to 2.1 - 2.4 m in April, ~10-40 cm thicker than our snow depths but with a similar overall decline of ~10-30 cm depending on the month analysed, with 2020-2021 notably thinner.

3.3.1 Key drivers of winter thickness differences

The regional anomaly maps allude to a strong ice type dependency as some of the more significant winter anomalies are observed within the thicker/older ice of the Central Arctic. To explore this further, Figures 14 and 15 show the seasonal timeseries of IS2SITMOGR4 v2 but delineated by ice type (data still masked outside the Inner Arctic Ocean domain). Figure 14 shows the mean seasonal time series of regions identified as first-year ice (FYI) only. The differences in FYI freeboard and snow depth in November/December are small (<1 cm) across the three winters, with the higher 2018-2019 FYI freeboard and snow depth only appearing later in the season compared to the 'all ice' analysis (Figure 13). The resultant FYI sea ice thickness winter timeseries comparison is notable for its consistency across the three winters (interannual thickness differences < 15 cm across all months).

Figure 15 shows the mean seasonal time series of regions identified as multiyear ice (MYI) only. The interannual MYI differences across most variables are higher than the FYI differences. The 2018 November MYI freeboards are 5 cm higher than the 2019 and 2020 Novembers. These freeboard difference largely persists until February onwards when the 2019-2020 freeboard increases and reduces the interannual spread, driven by the coincident strong increase in 2019-2020 snow depths. The result is MYI thickness that exhibits similar seasonal cycles across the three winters but with differences of 10 to 50 cm across the years that largely persist across the three winters with each year thinner than the one before. The result is 2020-2021 winter Arctic MYI thicknesses that are ~ 50 cm lower than the 2018-2019 winter. This 50 cm MYI thickness decline in just this three year period was also highlighted in Kacimi and Kwok, (2022).

These ice type differences align with our general understanding of winter sea ice growth – thinner ice is more responsive to atmospheric forcing and can thicken rapidly due to its reduced insulation (the negative feedback of ice growth) so small differences in the thickness of thin FYI at the start of winter are not expected to be good predictors of end-of-winter thickness (Petty et al., 2018b). Conversely, MYI is significantly thicker at the start of winter, meaning thickness anomalies are more likely to persist through winter as the ice is more insulated and less sensitive to atmospheric forcing. The differences in MYI thickness at the start of our three winters appears to provide a strong control on the total (combined MYI and FYI) winter thickness anomalies across all months, albeit in this limited record. Previous studies based on CryoSat-2 derived Arctic sea ice thickness estimates have highlighted the significant role of variable summer conditions in determining start of winter ice thickness anomalies and thus total winter thickness (and volume) anomalies (Tilling et al., 2015; Kwok, 2015). More specifically, a sharp increase in the start-of-winter 2013 Arctic thickness/volume was related to reductions in the duration of the summer melt season (Tilling et al., 2015) and also to dynamically driven convergence of ice within the Central Arctic (Kwok, 2015). The observed positive autumn 2013 thickness anomaly persisted through winter months, as in

our 2018/2019 results. We do not seek to provide a similar level of analysis in this study as our primary goal was to highlight and describe this new thickness dataset, but the agreement with our prior physical understanding is encouraging.

To better understand some of the more regional differences, the spatial thickness maps in Figure 11 include winter mean ice drifts from the monthly OSI SAF global low resolution ice drift product (Lavergne et al., 2010). In general, the mean circulation across these three winters are similar – featuring anti-clockwise Beaufort Gyre circulations and Transpolar drifts, but with some key differences. For example, ice drifts through the southern Beaufort Sea in 2018-2019 winter were stronger than the 2019-2020 and 2020-2021 drifts, which is likely associated with the positive freeboard/snow depth/thickness anomalies observed in the Chukchi Sea and negative anomalies in the Beaufort Sea in 2018-2019. Disentangling cause from effect is challenging as ice drift is strongly influenced by the sea ice conditions (Petty et al., 2016), however the strong association between drift patterns and thickness anomalies is again encouraging. Stronger ice drift anomalies are apparent when assessing monthly (not seasonal) differences, which can be explored more in the relevant Jupyter Book page (https://nicolekeeney.com/icesat2-book/sea_ice_characteristics).

Finally, to briefly explore any possible winter atmospheric drivers of these differences, Figure 16 shows an analysis of ERA5 near-surface (2 m) air temperature and downwelling longwave radiation over our Inner Arctic Ocean domain. The 2018-2019 winter shows lower temperatures and downward longwave flux at the start of winter (November through January) compared to 2019-2020 and 2020-2021, but higher temperatures and downward longwave flux in the middle-end of winter (February and March) compared to the following winters. April temperatures and downward longwave are similar in 2018-20919 to 2019-2020. It has been well-established that near-surface atmospheric conditions are strongly coupled to variability in the sea ice state so, as in the ice drift analysis, it is challenging to differentiation cause from effect. Nevertheless, our limited three-year analysis provides some limited evidence of the link between near-surface atmospheric conditions during the start-middle of winter and interannual winter ice conditions, promoting persistence of the interannual start-of-winter thickness anomalies (especially for the thicker MYI). The atmospheric analysis can be viewed and explored more in the relevant Jupyter Book page (https://nicolekeeney.com/icesat2-book/atmospheric_variables). A longer time-series, ideally complemented by fully coupled climate model studies, is needed to explore these relationships in more detail.

4 Summary

In this study we provided an impact assessment of upgrades to the input data used to produce ICESat-2-derived winter Arctic sea ice thickness estimates shown in Petty et al., (2020), and an extended analysis of the upgraded monthly gridded winter Arctic thickness dataset across the three winters profiled since the launch of ICESat-2 in September 2018.

Input data upgrades include the ICESat-2 ATL10 freeboards (Release 002 to 005, rel002 to rel005) and NASA Eulerian Snow On Sea Ice Model (NESOSIM, version 1.0 to version 1.1) snow loading. A key change in ATL10 data was the removal of misclassified leads from the determination of sea surface and thus freeboard in rel003. This was thought to be the primary cause of the increase in freeboard observed in January 2019 and April 2019 in rel003 data compared to rel002,

together with the more significant primary peak of lower freeboards in November 2018 rel003 data. The rel005-derived monthly gridded winter Arctic ice thickness data show improved comparisons with thickness estimates produced from ESA's CryoSat-2 using the same input assumptions across all 2018-2019 winter months (lower mean biases and standard deviations, higher correlations) compared to rel002-derived estimates. Later releases of ATL10 (rel004 and rel005) involved only minor changes to the freeboard algorithms and thus exhibit less significant changes in the observed freeboard distributions compared to the rel002 to rel003 change. The different releases also show slight differences in ATL10 data coverage, due primarily to the changes associated with dark lead usage, but also the inclusion/filtering of satellite calibration scan data. Our updated version 2 monthly gridded winter Arctic sea ice thickness dataset now utilizes all three strong beams to help mitigate these coverage issues and includes preliminary interpolated/smoothed data variables.

Our upgraded version of NESOSIM (version 1.1) presented in this study includes a new wind-driven atmosphere snow loss term, CloudSat-scaled ERA5 snowfall forcing (Cabaj et al., 2020) and some more minor bug fixes. NESOSIM v1.1 was also re-calibrated (heuristically) using spring Arctic snow depth estimates obtained by NASA's Operation IceBridge airborne mission (a gridded consensus product derived in this study). NESOSIM v1.1 generally shows similar snow depths to NESOSIM v1.0, resulting in a less significant impact on Arctic winter sea ice thickness compared to the rel002 to rel003 freeboard changes. A new NESOSIM v1.1 modern-era mean output was produced from 2010-2020 daily means towards the production of a more near-real time thickness retrievals from the forthcoming Quick Look ATL10 freeboard dataset.

Finally, we presented estimates of winter Arctic sea ice thickness from this updated monthly gridded winter Arctic sea ice thickness dataset (IS2SITMOGR4 v2) over the past three winter seasons of data collection (November 2018 – April 2021, September 2019 - April 2020 and September 2020 – April 2021). Our results showed clear differences in mean winter Arctic sea ice thickness within our Inner Arctic Ocean domain across the three winters profiled, due primarily to differences in the multiyear ice thickness across the three winters (multiyear ice thinning of 10 to 50 cm each year across the three winters analysed). Interannual changes in snow depth provide significant regional/monthly impacts on our thickness results – mitigating some, or in some cases all, of the impact from interannual differences in Arctic winter freeboards observed by ICESat-2.

Our results provide further evidence of the importance of accurate snow representation when assessing interannual variability in winter Arctic sea ice thickness from satellite altimetry (Bunzel et al., 2018; Mallett et al., 2021). Specific regional thickness anomalies, e.g., in the Southern Beaufort and Chukchi seas, were associated with interannual ice drift anomalies. Our mean Inner Arctic Ocean thickness estimates showed good agreement with those generated from the PIOMAS v2.1 reanalysis in terms of the seasonal cycle and interannual differences, although more significant differences were noted at regional scales.

4.1 Future work

ICESat-2/ATL10: Work is still on-going to re-introduce dark leads to the sea surface and freeboard algorithm in ATL10, which requires a new filter to skilfully discriminate dark lead segments (low photon rate) from segments with photon attenuation driven by the presence of clouds. The variable properties of clouds and their impact on photon attenuation, together with the limited availability of coincident imagery for validation (as used in Petty et al., 2021) makes this development challenging. An additional near-term goal related to ATL10 is the plan to utilize all six beams, or at least the three strong beams, concurrently to produce two-dimensional interpolated fields of sea surface height, as opposed to the independent beam processing currently utilized. However, residual absolute height biases of several centimetres are still observed between the beams as of Release 005 (updated from the analysis shown in Bagnardi et al., 2021, not shown), hindering this development. More sophisticated sea surface interpolation methods should also be explored (Landy et al., 2021). Algorithm development efforts related to these issues are on-going through the ICESat-2 Project Science Office to be included in future ATL10 data releases.

Snow loading: Work is on-going to utilize a Markov Chain Monte Carlo (MCMC) approach to automate the calibration of NESOSIM and provide a more robust uncertainty estimate of snow depth and density from this simple model framework (Cabaj et al., 2021). This approach benefits from the low computational cost of NESOSIM, allowing thousands of model simulations to be generated across plausible model parameter space. Additional physical upgrades are still desired, e.g., the introduction of a snow melt parameterization to extend NESOSIM through summer. However, additional reliable ground-truth data at regional/basin-scales are needed to calibrate and validate such development activities.

Recent studies leveraging newly generated Arctic snow reconstructions and satellite-derived data products, including the joint ICESat-2/CryoSat-2 derived snow depths, are helping collectively provide new insights into snow depth variability and its impacts on sea ice thickness and its contribution to total thickness uncertainty (Zhou et al., 2021; Mallett et al., 2021; Glissenaar et al., 2021; Kacimi and Kwok, 2022). While these datasets, including NESOSIM, are still generally limited by a lack of contemporary ground-truth data for assessing data accuracy, the creation of new operational, i.e., continuously updated and disseminated, snow products should help enable more comprehensive assessments of systematic snow loading uncertainties.

ICESat-2-derived sea ice thickness: Our primary focus of the three-winter thickness assessment was the monthly gridded winter Arctic thickness dataset (IS2SITMOGR4 v2, Petty et al., 2022b). However, raw (and 10 km smoothed) along-track data at the segment resolution of ATL10 (~20 m) are also available (IS2SITDAT4, Petty et al., 2022a, data shown in Figure 7), which provide higher fidelity information regarding the sea ice state than the monthly gridded estimates. Work is currently on-going to assess the winter Arctic sea ice thickness distribution from these data including comparisons with model-based estimates. Continued refinement and/or redevelopment of the snow redistribution scheme is expected. We also hope to combine these data with new ICESat-2-derived floe size estimates (Petty et al., 2021) towards a joint floe size-thickness distribution in combination with efforts to improve the accuracy of the lead/ice discrimination. The along-track

dataset is more computationally demanding but increasing access to high performance computing environments (e.g., cloud compute platforms) would help increase its usability. The extension of NESOSIM through summer months will help enable summer preliminary production of summer Arctic thickness estimates.

Sea ice thickness reconciliation: The improved correspondence between our ICESat-2 derived estimates of winter Arctic sea ice thickness and those generated from ESA's CryoSat-2 are encouraging. There are clear advantages (and disadvantages) from estimating sea ice thickness from either radar or laser altimetry, which need to be better considered and utilized for constraining total Arctic, and eventually Antarctic, sea ice volume. Radar altimeters, e.g., CryoSat-2, are highly sensitive to leads and are unaffected by clouds, providing benefits to both the quality and coverage of data collected. In contrast, laser altimeters (e.g., ICESat/ICESat-2) generally provide higher resolution data and obtain more precise estimates of the snow-covered ice surface height (and thus total freeboard) compared to the arguably less distinct/certain ice-snow interface height (and thus ice freeboard) obtained by typical radar altimeters. The effective radar penetration depth at *Ku/Ka*-band is generally considered to come from the ice-snow interface although recent studies continue to challenge this (Nandan et al., 2017, King et al., 2018). In both cases, uncertainties in the derived freeboard estimates are combined with uncertainties in the various input assumptions (snow loading, sea ice density) to provide total thickness uncertainty estimates. Constraining the various input uncertainties and residual biases remains challenging, which points to the need for improved exploitation of existing ground-truth data and further field and airborne campaigns considering the fast-changing Arctic. The good agreement between our results and those of Kwok and Kacimi (2022) using joint ICESat-2 and CryoSat-2 processing is also encouraging, but significant differences are still observed at more regional scales that is worthy of further investigation. Improvements to the underlying freeboard algorithms and input assumptions are urgently needed as we seek to reconcile these datasets and hopefully move towards multi-sensor thickness assessments (increasing coverage and data quality). Planning is underway for a coordinated intercomparison exercise around new semi-synchronous along-track measurements available since the CRYO2ICE orbit alignment (https://earth.esa.int/eogateway/missions/cryosat/cryo2ice).

Code availability

Our analysis of the monthly gridded winter Arctic thickness data described above (Figures 10-16) have been summarized and made available through an online Jupyter Book (https://nicolekeeney.com/icesat2-book/home.html). Interested users are able to view the various figures (and additional plots not shown here), view the code used to generate them, and also interactively run the analysis locally or online (using the associated Binder links, https://mybinder.org), e.g., changing the domain and/or months of interest. It is our expectation that this Jupyter Book will be updated as new IS2SITMOGR4 data are created and made public to enable continued assessments of winter Arctic thickness change. A version tagged version of this Jupyter Book will be obtained and archived on Zenodo on completion of peer review.

NESOSIM is available on GitHub (https://github.com/akpetty/NESOSIM/) and the version 1.1 release used in this study has been tagged as a specific release on GitHub and archived on Zenodo (https://doi.org/10.5281/zenodo.4448356).

The original sea ice thickness processing code presented in Petty et al., (2020) is available on GitHub (https://github.com/akpetty/ICESat-2-sea-ice-thickness, all in the open-source language Python). We plan to update this using the small upgrades made to our processing chain on completion of this peer-review.

Data availability

The monthly gridded winter Arctic sea ice thickness data derived in this study (IS2SITMOGR4, version 2) is being made available through the National Snow and Ice Data Center (NSIDC) (https://nsidc.org/data/IS2SITMOGR4, Petty et al., 2022b). The along-track (raw and 10 km mean) Arctic sea ice thickness estimates are also in the process of being ingested and made publicly available through the NSIDC (IS2SITDAT4, https://nsidc.org/data/IS2SITDAT4, Petty et al., 2022a).

The ICESat-2 ATL10 sea ice freeboard data (currently Release 005) can be obtained from the NSIDC (https://nsidc.org/data/atl10). NSIDC generally maintains an archive of ICESat-2 data from the current and previous release, so currently Release 004 can be obtained from the NSIDC also (https://nsidc.org/data/atl10/versions/4).

The output from our NESOSIM v1.1 model framework from 1980-2021 and the NESOSIM v1.1 climatology presented here has been archived on Zenodo (https://doi.org/10.5281/zenodo.5164314).

Daily and monthly NASA Climate Data Record (CDR) version 4 ice concentration data were obtained from the NSIDC (https://nsidc.org/data/G02202). ERA5 estimates of daily snowfall, winds and near surface temperature and downwelling longwave radiation were obtained from the European Centre for Medium-Range Weather Forecasts (ECMWF) Copernicus Climate Change Service Climate Data Store (https://cds.climate.copernicus.eu). EUMETSAT OSI SAF ice motion data were obtained through their web portal (http://osisaf.met.no/p/ice/, last access: 1 May 2021). OSI SAF ice type data were obtained from their ftp repository (ftp://osisaf.met.no/prod/ice/type/, last access 1 May 2021). Polar Pathfinder version 4 ice drifts were obtained from the NSIDC (https://nsidc.org/data/nsidc-0116/versions/4).

The NASA GSFC CryoSat-2 (CS-2) Arctic sea ice thickness data were obtained from the NSIDC (https://nsidc.org/data/RDEFT4, last access: 1 May 2019). The CPOM CS-2 thickness data were obtained from their web portal (http://www. cpom.ucl.ac.uk/csopr/seaice.html, last access: 1 May 2019). The AWI CS-2 thickness data were obtained from their web portal (http://data.seaiceportal.de/data/cryosat2/version2.1/l3c_grid, last access: 1 May 2019). The NASA JPL CS-2 thickness data were obtained directly from Dr. Ron Kwok.

Author contributions

AP led the study, produced the updated NESOSIM v1.1 framework/output and ICESat-2 thickness estimates (along-track and gridded). NK produced the Jupyter Book with assistance from AP and helped produce the new interpolated thickness variables. AC and PK worked with AP to produce the updated NESOSIM v1.1. framework and output. MB generated the

release and beam coverage assessments and provided key input on ATL10 upgrades. AP wrote the manuscript with input/edits provided from all authors.

Competing interests

The authors declare that they have no conflict of interest.

Acknowledgements

We would like to thank the ICESat-2 scientists and engineers for their continued efforts in enabling the production of the high-quality freeboard data analysed in this study. Thanks also to the NSIDC team for their continued support in documenting and hosting our derived winter Arctic sea ice thickness data.

References

Bagnardi, M., Kurtz, N. T., Petty, A. A., and Kwok, R.: Sea Surface Height Anomalies of the Arctic Ocean From ICESat-2: A First Examination and Comparisons With CryoSat-2, 48, e2021GL093155, https://doi.org/10.1029/2021GL093155, 2021.

Barrett, A. P., Stroeve, J. C., and Serreze, M. C.: Arctic Ocean Precipitation From Atmospheric Reanalyses and Comparisons With North Pole Drifting Station Records, 125, e2019JC015415, https://doi.org/10.1029/2019JC015415, 2020.

Breivik, L. A., Eastwood, S., and Lavergne, T.: Use of C-Band Scatterometer for Sea Ice Edge Identification, 50, 2669–2677, https://doi.org/10.1109/TGRS.2012.2188898, 2012.

Bunzel, F., Notz, D., and Pedersen, L. T.: Retrievals of Arctic Sea-Ice Volume and Its Trend Significantly Affected by Interannual Snow Variability, 45, 11,751-11,759, https://doi.org/10.1029/2018GL078867, 2018.

Cabaj, A., Kushner, P. J., Fletcher, C. G., Howell, S., and Petty, A. A.: Constraining Reanalysis Snowfall Over the Arctic Ocean Using CloudSat Observations, 47, e2019GL086426, https://doi.org/10.1029/2019GL086426, 2020.

Community, S.: Arctic Sea Ice in CMIP6, 47, e2019GL086749, https://doi.org/10.1029/2019GL086749, 2020.

Dee, D. P., Uppala, S. M., Simmons, A. J., Berrisford, P., Poli, P., Kobayashi, S., Andrae, U., Balmaseda, M. A., Balsamo, G., Bauer, P., Bechtold, P., Beljaars, A. C. M., van de Berg, L., Bidlot, J., Bormann, N., Delsol, C., Dragani, R., Fuentes, M., Geer, A. J., Haimberger, L., Healy, S. B., Hersbach, H., Holm, E. V., Isaksen, L., Kallberg, P., Kahler, M., Matricardi, M., McNally, A. P., Monge-Sanz, B. M., Morcrette, J.-J., Park, B.-K., Peubey, C., de Rosnay, P., Tavolato, C., Thepaut, J.-N., and Vitart, F.: The ERA-Interim reanalysis: configuration and performance of the data assimilation system, 137, 553–597, https://doi.org/10.1002/qj.828, 2011.

Giles, K. A., Laxon, S. W., Wingham, D. J., Wallis, D. W., Krabill, W. B., Leuschen, C. J., McAdoo, D., Manizade, S. S., and Raney, R. K.: Combined airborne laser and radar altimeter measurements over the Fram Strait in May 2002, Remote Sensing of Environment, 111, 182–194, https://doi.org/10.1016/j.rse.2007.02.037, 2007.

Glissenaar, I. A., Landy, J. C., Petty, A. A., Kurtz, N. T., and Stroeve, J. C.: Impacts of snow data and processing methods on the interpretation of long-term changes in Baffin Bay early spring sea ice thickness, 15, 4909–4927, https://doi.org/10.5194/tc-15-4909-2021, 2021.

Granskog, M. A., Rösel, A., Dodd, P. A., Divine, D., Gerland, S., Martma, T., and Leng, M. J.: Snow contribution to first-year and second-year Arctic sea ice mass balance north of Svalbard, 122, 2539–2549, https://doi.org/10.1002/2016JC012398, 2017.

Hendricks, S. and Ricker, R.: User guide—AWI CryoSat-2 sea ice thickness data product (v1.2). Retrieve from http://epic.awi.de/ 41242/, 2016.

Hersbach, H., Bell, B., Berrisford, P., Hirahara, S., Horányi, A., Muñoz-Sabater, J., Nicolas, J., Peubey, C., Radu, R., Schepers, D., Simmons, A., Soci, C., Abdalla, S., Abellan, X., Balsamo, G., Bechtold, P., Biavati, G., Bidlot, J., Bonavita, M., De Chiara, G., Dahlgren, P., Dee, D., Diamantakis, M., Dragani, R., Flemming, J., Forbes, R., Fuentes, M., Geer, A., Haimberger, L., Healy, S., Hogan, R. J., Hólm, E., Janisková, M., Keeley, S., Laloyaux, P., Lopez, P., Lupu, C., Radnoti, G., de Rosnay, P., Rozum, I., Vamborg, F., Villaume, S., and Thépaut, J.-N.: The ERA5 global reanalysis, 146, 1999–2049, https://doi.org/10.1002/qj.3803, 2020.

Kacimi, S. and Kwok, R.: Arctic Snow Depth, Ice Thickness, and Volume From ICESat-2 and CryoSat-2: 2018–2021, 49, e2021GL097448, https://doi.org/10.1029/2021GL097448, 2022.

King, J., Howell, S., Derksen, C., Rutter, N., Toose, P., Beckers, J. F., Haas, C., Kurtz, N., and Richter-Menge, J.: Evaluation of Operation IceBridge quick-look snow depth estimates on sea ice, Geophys. Res. Lett., 42, 2015GL066389, https://doi.org/10.1002/2015GL066389, 2015.

King, J., Skourup, H., Hvidegaard, S. M., Rösel, A., Gerland, S., Spreen, G., Polashenski, C., Helm, V., and Liston, G. E.: Comparison of Freeboard Retrieval and Ice Thickness Calculation From ALS, ASIRAS, and CryoSat-2 in the Norwegian Arctic, to Field Measurements Made During the N-ICE2015 Expedition, J. Geophys. Res. Oceans, n/a-n/a, https://doi.org/10.1002/2017JC013233, n.d.

Koenig, L. S., Ivanoff, A., Alexander, P. M., MacGregor, J. A., Fettweis, X., Panzer, B., Paden, J. D., Forster, R. R., Das, I., McConnell, J. R., Tedesco, M., Leuschen, C., and Gogineni, P.: Annual Greenland accumulation rates (2009–2012) from airborne snow radar, The Cryosphere, 10, 1739–1752, https://doi.org/10.5194/tc-10-1739-2016, 2016.

Kurtz, J. C. and Harbeck, J.: CryoSat-2 Level 4 Sea Ice Elevation, Freeboard, and Thickness, Version 1. Boulder, Colorado USA: NASA DAAC at the National Snow and Ice Data Center, https://doi.org/0.5067/96JO0KIFDAS8, 2017.

Kurtz, N. T., Markus, T., Cavalieri, D. J., Sparling, L. C., Krabill, W. B., Gasiewski, A. J., and Sonntag, J. G.: Estimation of sea ice thickness distributions through the combination of snow depth and satellite laser altimetry data, J. Geophys. Res., 114, C10007, https://doi.org/10.1029/2009JC005292, 2009.

Kurtz, N. T., Farrell, S. L., Studinger, M., Galin, N., Harbeck, J. P., Lindsay, R., Onana, V. D., Panzer, B., and Sonntag, J. G.: Sea ice thickness, freeboard, and snow depth products from Operation IceBridge airborne data, 7, 1035–1056, https://doi.org/10.5194/tc-7-1035-2013, 2013.

Kwok, R.: Sea ice convergence along the Arctic coasts of Greenland and the Canadian Arctic Archipelago: Variability and extremes (1992–2014), 42, 7598–7605, https://doi.org/10.1002/2015GL065462, 2015.

Kwok, R.: Arctic sea ice thickness, volume, and multiyear ice coverage: losses and coupled variability (1958–2018), Environ. Res. Lett., 13, 105005, https://doi.org/10.1088/1748-9326/aae3ec, 2018.

Kwok, R. and Cunningham, G. F.: ICESat over Arctic sea ice: Estimation of snow depth and ice thickness, J. Geophys. Res., 113, C08010, https://doi.org/10.1029/2008JC004753, 2008.

Kwok, R. and Cunningham, G. F.: Variability of Arctic sea ice thickness and volume from CryoSat-2, 373, https://doi.org/10.1098/rsta.2014.0157, 2015.

Kwok, R., Cunningham, G. F., Hoffmann, J., and Markus, T.: Testing the ice-water discrimination and freeboard retrieval algorithms for the ICESat-2 mission, Remote Sensing of Environment, 183, 13–25, https://doi.org/10.1016/j.rse.2016.05.011, 2016.

Kwok, R., Kurtz, N. T., Brucker, L., Ivanoff, A., Newman, T., Farrell, S. L., King, J., Howell, S., Webster, M. A., Paden, J., Leuschen, C., MacGregor, J. A., Richter-Menge, J., Harbeck, J., and Tschudi, M.: Intercomparison of snow depth retrievals over Arctic sea ice from radar data acquired by Operation IceBridge, 11, 2571–2593, https://doi.org/10.5194/tc-11-2571-2017, 2017.

Kwok, R., Kacimi, S., Markus, T., Kurtz, N. T., Studinger, M., Sonntag, J. G., Manizade, S. S., Boisvert, L. N., and Harbeck, J. P.: ICESat-2 surface height and sea-ice freeboard assessed with ATM lidar acquisitions from Operation IceBridge, 44, 11228–11236, https://doi.org/10.1029/2019GL084976, 2019a.

Kwok, R., Markus, T., Kurtz, N. T., Petty, A. A., Neumann, T. A., Farrell, S. L., Cunningham, G. F., Hancock, D. W., Ivanoff, A., and Wimert, J. T.: Surface Height and Sea Ice Freeboard of the Arctic Ocean From ICESat-2: Characteristics and Early Results, 124, 6942–6959, https://doi.org/10.1029/2019JC015486, 2019b.

Kwok, R., Petty, A., Cunningham, G., Markus, T., Hancock, D., Ivanoff, A., Wimert, J., Bagnardi, M., and Kurtz, N.: ATLAS/ICESat-2 L3A Sea Ice Freeboards, Version 5, https://doi.org/10.5067/ATLAS/ATL10.005, 2021a.

Kwok, R., Petty, A., Cunningham, G., Markus, T., Hancock, D., Ivanoff, A., Wimert, J., Bagnardi, M., and Kurtz, N.: ATLAS/ICESat-2 L3A Sea Ice Heights, Version 5, https://doi.org/10.5067/ATLAS/ATL07.005, 2021b.

Kwok, R., Petty, A., Wimert, J., Bagnardi, M., Cuningham, G., Hancock, D., Ivanoff, A., and Kurtz, N.: Ice, Cloud, and Land Elevation Satellite-2 Project: Algorithm Theoretical Basis Document (ATBD) for Sea Ice Products, Release 005, https://icesat-2.gsfc.nasa.gov/science/data-products, 2021c.

Kwok, R., Petty, A. A., Bagnardi, M., Kurtz, N. T., Cunningham, G. F., Ivanoff, A., and Kacimi, S.: Refining the sea surface identification approach for determining freeboards in the ICESat-2 sea ice products, 15, 821–833, https://doi.org/10.5194/tc-15-821-2021, 2021d.

Labe, Z., Magnusdottir, G., and Stern, H.: Variability of Arctic sea-ice thickness using PIOMAS and the CESM Large Ensemble, J. Climate, https://doi.org/10.1175/JCLI-D-17-0436.1, 2018.

Landy, J. C., Bouffard, J., Wilson, C., Rynders, S., Aksenov, Y., and Tsamados, M.: Improved Arctic Sea Ice Freeboard Retrieval From Satellite Altimetry Using Optimized Sea Surface Decorrelation Scales, 126, e2021JC017466, https://doi.org/10.1029/2021JC017466, 2021.

Lavergne, T., Eastwood, S., Teffah, Z., Schyberg, H., and Breivik, L.-A.: Sea ice motion from low-resolution satellite sensors: An alternative method and its validation in the Arctic, J. Geophys. Res., 115, C10032, https://doi.org/10.1029/2009JC005958, 2010.

Laxon, S. W., Giles, K. A., Ridout, A. L., Wingham, D. J., Willatt, R., Cullen, R., Kwok, R., Schweiger, A., Zhang, J., Haas, C., Hendricks, S., Krishfield, R., Kurtz, N., Farrell, S., and Davidson, M.: CryoSat-2 estimates of Arctic sea ice thickness and volume, 40, 732–737, https://doi.org/10.1002/grl.50193, 2013.

Liston, G. E., Itkin, P., Stroeve, J., Tschudi, M., Stewart, J. S., Pedersen, S. H., Reinking, A. K., and Elder, K.: A Lagrangian Snow-Evolution System for Sea-Ice Applications (SnowModel-LG): Part I—Model Description, 125, e2019JC015913, https://doi.org/10.1029/2019JC015913, 2020.

Magruder, L. A., Brunt, K. M., and Alonzo, M.: Early ICESat-2 on-orbit Geolocation Validation Using Ground-Based Corner Cube Retro-Reflectors, 12, 3653, https://doi.org/10.3390/rs12213653, 2020.

Mallett, R. D. C., Stroeve, J. C., Tsamados, M., Landy, J. C., Willatt, R., Nandan, V., and Liston, G. E.: Faster decline and higher variability in the sea ice thickness of the marginal Arctic seas when accounting for dynamic snow cover, 15, 2429–2450, https://doi.org/10.5194/tc-15-2429-2021, 2021.

Markus, T., Neumann, T., Martino, A., Abdalati, W., Brunt, K., Csatho, B., Farrell, S., Fricker, H., Gardner, A., Harding, D., Jasinski, M., Kwok, R., Magruder, L., Lubin, D., Luthcke, S., Morison, J., Nelson, R., Neuenschwander, A., Palm, S., Popescu, S., Shum, C., Schutz, B. E., Smith, B., Yang, Y., and Zwally, J.: The Ice, Cloud, and land Elevation Satellite-2 (ICESat-2): Science requirements, concept, and implementation, Remote Sensing of Environment, 190, 260–273, https://doi.org/10.1016/j.rse.2016.12.029, 2017.

Meier, W. N., Fetterer, F., Savoie, M., Mallory, S., Duerr, R., and Stroeve, J.: NOAA/NSIDC Climate Data Record of Passive Microwave Sea Ice Concentration, Version 3, https://doi.org/10.7265/N59P2ZTG, 2017.

Meier, W. N., Fetterer, F., Windnagel, A. K., and Stewart, J. S.: NOAA/NSIDC Climate Data Record of Passive Microwave Sea Ice Concentration, Version 4 [September 2018 to April 2021], https://doi.org/10.7265/efmz-2t65, 2021.

Moore G. W. K., Schweiger A., Zhang J., and Steele M.: Collapse of the 2017 Winter Beaufort High: A Response to Thinning Sea Ice?, Geophysical Research Letters, 0, https://doi.org/10.1002/2017GL076446, 2018.

Nandan, V., Geldsetzer, T., Yackel, J., Mahmud, M., Scharien, R., Howell, S., King, J., Ricker, R., and Else, B.: Effect of Snow Salinity on CryoSat-2 Arctic First-Year Sea Ice Freeboard Measurements, 44, 10,419-10,426, https://doi.org/10.1002/2017GL074506, 2017.

Neumann, T. A., Martino, A. J., Markus, T., Bae, S., Bock, M. R., Brenner, A. C., Brunt, K. M., Cavanaugh, J., Fernandes, S. T., Hancock, D. W., Harbeck, K., Lee, J., Kurtz, N. T., Luers, P. J., Luthcke, S. B., Magruder, L., Pennington, T. A., Ramos-Izquierdo, L., Rebold, T., Skoog, J., and Thomas, T. C.: The Ice, Cloud, and Land Elevation Satellite – 2 mission: A global geolocated photon product derived from the Advanced Topographic Laser Altimeter System, Remote Sensing of Environment, 233, 111325, https://doi.org/10.1016/j.rse.2019.111325, 2019.

Petty, A. A., Hutchings, J. K., Richter-Menge, J. A., and Tschudi, M. A.: Sea ice circulation around the Beaufort Gyre: The changing role of wind forcing and the sea ice state, J. Geophys. Res. Oceans, 121, 3278–3296, https://doi.org/10.1002/2015JC010903, 2016.

Petty, A. A., Webster, M., Boisvert, L., and Markus, T.: The NASA Eulerian Snow on Sea Ice Model (NESOSIM) v1.0: initial model development and analysis, 11, 4577–4602, https://doi.org/10.5194/gmd-11-4577-2018, 2018a.

Petty, A. A., Holland, M. M., Bailey, D. A., and Kurtz, N. T.: Warm Arctic, Increased Winter Sea Ice Growth?, 45, 12,922-12,930, https://doi.org/10.1029/2018GL079223, 2018b.

Petty, A. A., Kurtz, N. T., Kwok, R., Markus, T., and Neumann, T. A.: Winter Arctic Sea Ice Thickness From ICESat-2 Freeboards, 125, e2019JC015764, https://doi.org/10.1029/2019JC015764, 2020.

Petty, A. A., Bagnardi, M., Kurtz, N. T., Tilling, R., Fons, S., Armitage, T., Horvat, C., and Kwok, R.: Assessment of ICESat-2 Sea Ice Surface Classification with Sentinel-2 Imagery: Implications for Freeboard and New Estimates of Lead and Floe Geometry, 8, e2020EA001491, https://doi.org/10.1029/2020EA001491, 2021.

Petty, A. A., Kurtz, N., Kwok, R., Markus, T., and Neumann, T. A.: ICESat-2 L4 Along-Track Sea Ice Thickness, Version 1, https://doi.org/10.5067/JTI5YG3S6VAJ, 2022a.

Petty, A. A., Kurtz, N., Kwok, R., Markus, T., Neumann, T. A., and Keeney, N.: ICESat-2 L4 Monthly Gridded Sea Ice Thickness, Version 2, https://doi.org/10.5067/OE8BDP5KU30Q, 2022b.

Sallila, H., Farrell, S. L., McCurry, J., and Rinne, E.: Assessment of contemporary satellite sea ice thickness products for Arctic sea ice, 13, 1187–1213, https://doi.org/10.5194/tc-13-1187-2019, 2019.

Schweiger, A., Lindsay, R., Zhang, J., Steele, M., Stern, H., and Kwok, R.: Uncertainty in modeled Arctic sea ice volume, 116, https://doi.org/10.1029/2011JC007084, 2011.

Schweiger, A. J., Steele, M., Zhang, J., Moore, G. W. K., and Laidre, K. L.: Accelerated sea ice loss in the Wandel Sea points to a change in the Arctic's Last Ice Area, Commun Earth Environ, 2, 1–11, https://doi.org/10.1038/s43247-021-00197-5, 2021.

Stroeve, J., Liston, G. E., Buzzard, S., Zhou, L., Mallett, R., Barrett, A., Tschudi, M., Tsamados, M., Itkin, P., and Stewart, J. S.: A Lagrangian Snow Evolution System for Sea Ice Applications (SnowModel-LG): Part II—Analyses, 125, e2019JC015900, https://doi.org/10.1029/2019JC015900, 2020.

Tilling, R. L., Ridout, A., Shepherd, A., and Wingham, D. J.: Increased Arctic sea ice volume after anomalously low melting in 2013, 8, 643–646, https://doi.org/10.1038/ngeo2489, 2015.

Tilling, R. L., Ridout, A., and Shepherd, A.: Estimating Arctic sea ice thickness and volume using CryoSat-2 radar altimeter data, Advances in Space Research, 62, 1203–1225, https://doi.org/10.1016/j.asr.2017.10.051, 2018.

Tschudi, M., Meier, W., Stewart, J. S., Fowler, C., and Maslanik, J.: Polar Pathfinder Daily 25 km EASE-Grid Sea Ice Motion Vectors, Version 4. Boulder, Colorado USA. NASA National Snow and Ice Data Center Distributed Active Archive Center., https://doi.org/10.5067/INAWUWO7QH7B, 2019.

Wang, C., Graham, R. M., Wang, K., Gerland, S., and Granskog, M. A.: Comparison of ERA5 and ERA-Interim near-surface air temperature, snowfall and precipitation over Arctic sea ice: effects on sea ice thermodynamics and evolution, 13, 1661–1679, https://doi.org/10.5194/tc-13-1661-2019, 2019.

Warren, S. G., Rigor, I. G., Untersteiner, N., Radionov, V. F., Bryazgin, N. N., Aleksandrov, Y. I., and Colony, R.: Snow Depth on Arctic Sea Ice, J. Climate, 12, 1814–1829, https://doi.org/10.1175/1520-0442(1999)012<1814:SDOASI>2.0.CO;2, 1999.

Yu, Y., Xiao, W., Zhang, Z., Cheng, X., Hui, F., and Zhao, J.: Evaluation of 2-m Air Temperature and Surface Temperature from ERA5 and ERA-I Using Buoy Observations in the Arctic during 2010–2020, 13, 2813, https://doi.org/10.3390/rs13142813, 2021.

Zhou, L., Stroeve, J., Xu, S., Petty, A., Tilling, R., Winstrup, M., Rostosky, P., Lawrence, I. R., Liston, G. E., Ridout, A., Tsamados, M., and Nandan, V.: Inter-comparison of snow depth over Arctic sea ice from reanalysis reconstructions and satellite retrieval, 15, 345–367, https://doi.org/10.5194/tc-15-345-2021, 2021.

Zygmuntowska, M., Rampal, P., Ivanova, N., and Smedsrud, L. H.: Uncertainties in Arctic sea ice thickness and volume: new estimates and implications for trends, The Cryosphere, 8, 705–720, https://doi.org/10.5194/tc-8-705-2014, 2014.

Model parameter	NESOSIM v1.0	NESOSIM v1.1
New snow density, top layer (kg m^{-3})	200	200
Old snow density, bottom layer (kg m^{-3})	350	350
Wind action threshold (m s^{-1}), ω	5	5
Blowing snow open water loss coefficient (s^{-1}), $\boldsymbol{\beta}$	2.9×10^{-7}	1.45×10^{-7}
Blowing snow atmosphere loss coefficient (s^{-1}), $\boldsymbol{\gamma}$	N/A	2×10^{-8}
Wind packing coefficient, ω (s^{-1})	5.8×10^{-7}	5.8×10^{-7}
Forcing data		
Snowfall	MEDIAN-SF (Sep 2000 to Apr 2015) ERA-I (Sep 2018 to Apr 2019)	ERA5 (+ CloudSat scaling)
Near-surface winds	ERA-I	ERA5
Near-surface air temperature	ERA-I	ERA5
Sea ice concentration	Bootstrap (Sep 2000 to Apr 2015) NSIDC CDRv3 (Sep 2018-Apr 2019)	NSIDC CDR v3
Sea ice drift	NSIDC v3 (Sep 2000-Apr 2015) OSI SAF (Sep 2018-Apr 2019)	NSIDC v4 (Sep 1980 to April 2019) OSI SAF (Sep 2019 to Apr 2021)
Initial conditions		
Start date	August 15th	September 1st

Table 1: Model configurations for NESOSIM v1.0 and v1.1.

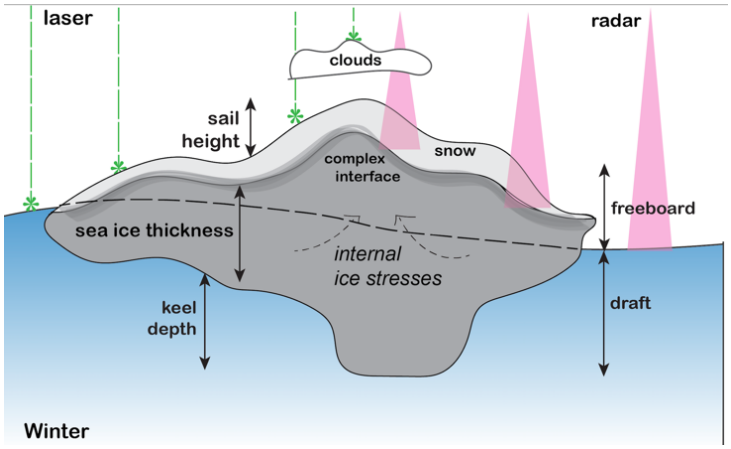

Figure 1: Schematic showing the typical approach and key challenges in active sea ice altimetry (laser, e.g., ICESat-2, radar, e.g., CryoSat-2) over sea ice.

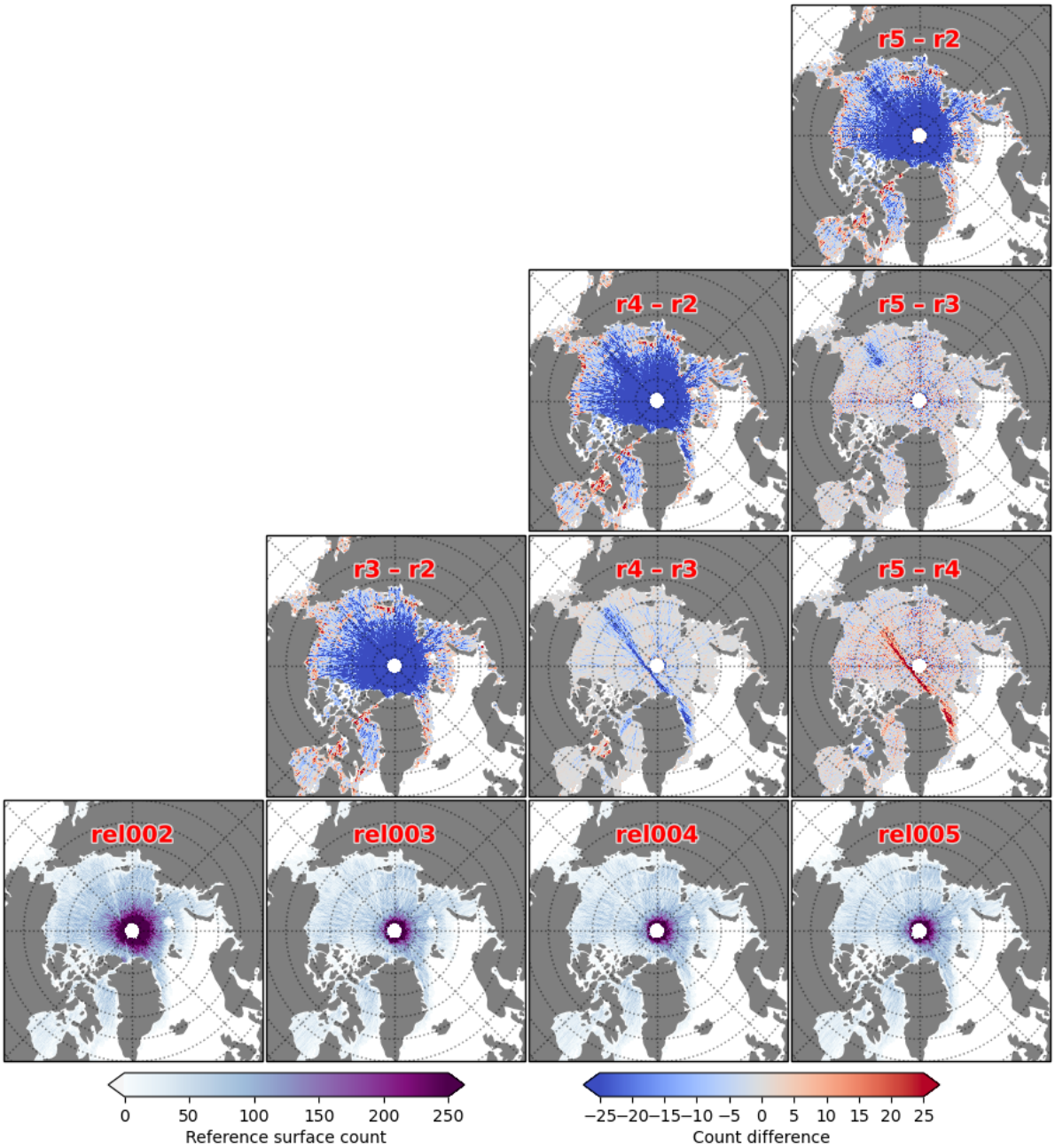

Figure 2: (bottom row) number of 10 km along-track reference surfaces from the three strong beams from November 2018 to April 2019 for Release 002/rel002 (left) to Release 005/rel005 (right). Panels above show the difference in reference surface counts between releases rel003 to rel005 relative to rel002.

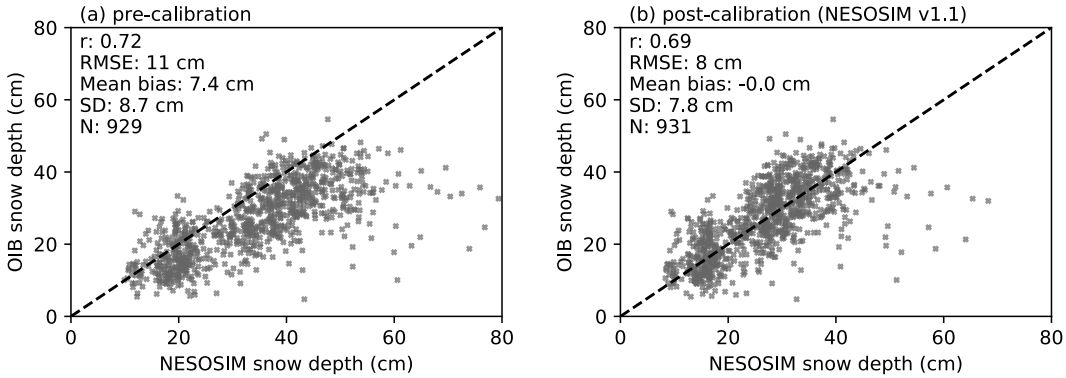

Figure 3: Comparison of (a) pre-calibration NESOSIM v1.1 and (b) post-calibration, NESOSIM v1.1 snow depths against spring (2010-2015) Arctic snow depths from gridded daily spring 2010 to 2015 median Operation IceBridge (OIB) snow depth estimates.

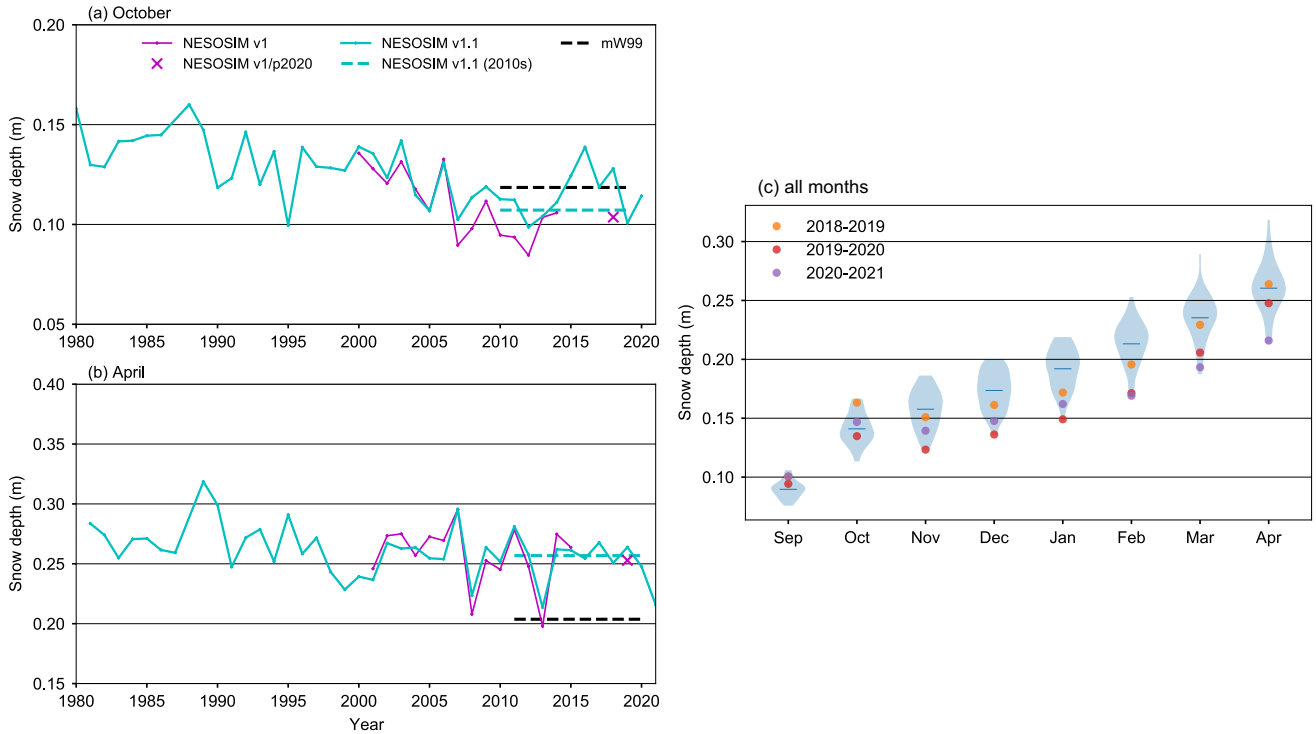

Figure 4: (Mean Arctic snow depths in October (a) and April (b) from NESOSIM v1.0 and v1.1 within an Inner Arctic Ocean domain (Figure 5). NESOSIM now depths are also masked where concentration (from passive microwave) is less than 25%. The cross markers show the extended ICESat-2 NESOSIM v1.0 results used in (Petty et al., 2020). The dashed cyan horizontal lines show the NESOSIMv1.1_2010-2020ave snow depths averaged across the respective month, while the dashed black lines show the modified Warren climatology (mW99) in October and April respectively for regions of coincident NESOSIM v1.1 coverage. (c) violin plots showing interannual distributions of monthly mean snow depths from NESOSIM v1.1 within an Inner Arctic Ocean domain from 1980-2021, colored markers indicate mean monthly snow depths for recent (ICESat-2) years.

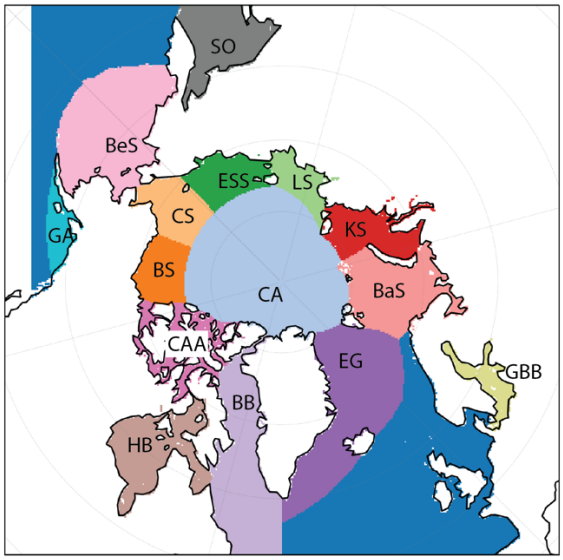

Figure 5: Region mask of the Arctic Ocean from the National Snow and Ice Data Center (NSIDC). CA: Central Arctic, BS: Beaufort Sea, CS: Chukchi Sea, ESS: East Siberian Sea, LS: Laptev Sea, KS: Kara Sea, BaS: Barents Sea, EG: East Greenland Sea, GBB: Gulf of Bothnia, Baltic Sea, BB: Baffin Bay & Davis Strait, BeS: Bering Sea, SO: Sea of Okhotsk, GA: Gulf of Alaska. The Inner Arctic Ocean domain used in the main manuscript is defined as the combined area of the Central Arctic, Beaufort Sea, Chukchi Sea, E Siberian Sea, Laptev Sea and Kara Sea. Data provided by W. Meier & S. Stewart.

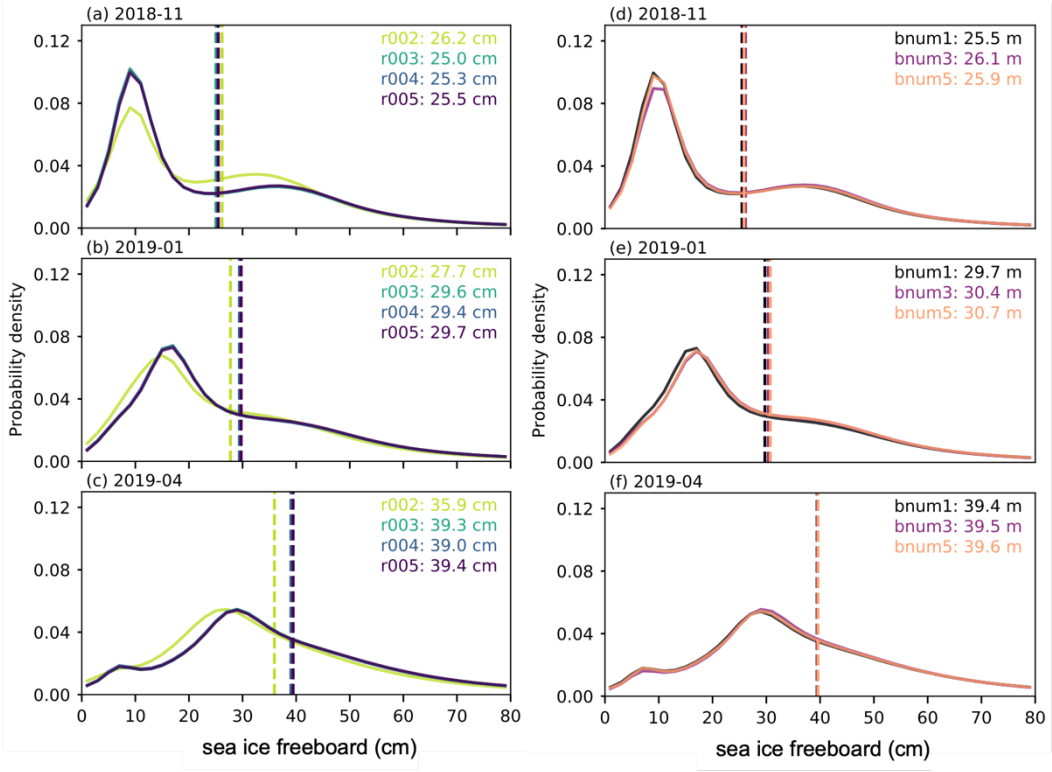

Figure 6: Probability distributions of ATL10 freeboard for (left column) Release 002 (rel002) to Release 005 (rel005) using strong beam #1 in November 2018, (top) January 2019 (middle) and April 2019 (bottom), and (right column) strong beam #1 #3 and #5 for Release 005 data.

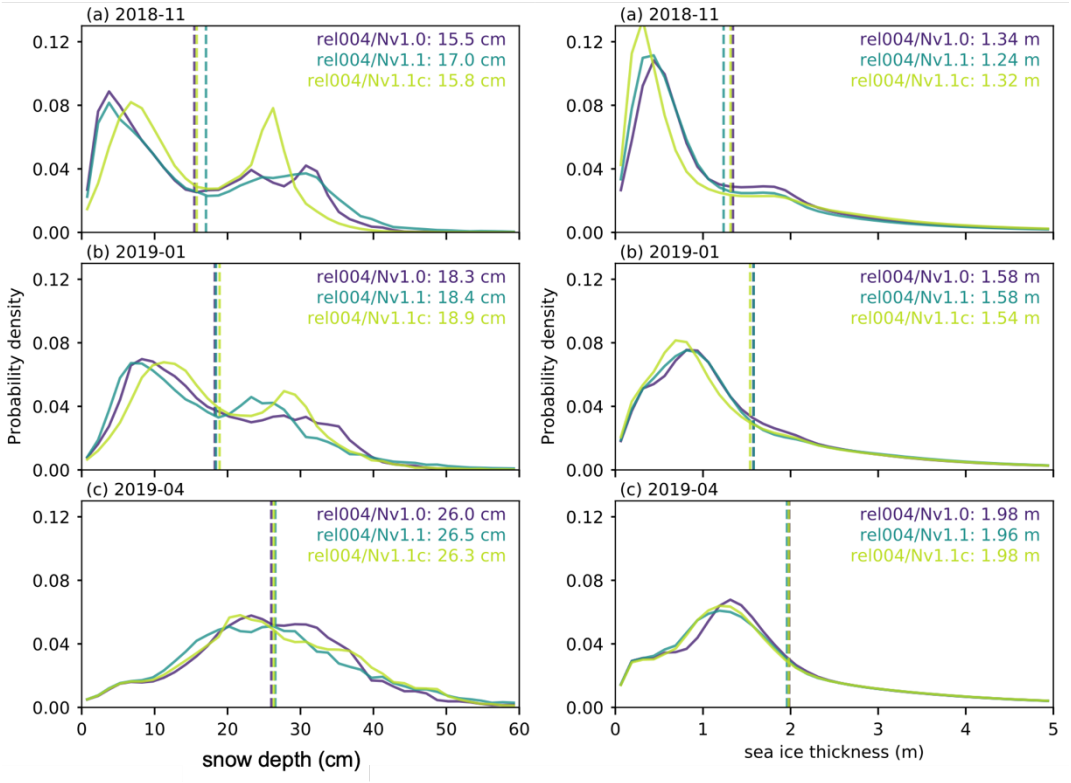

Figure 7: Probability distributions of (left column) redistributed snow depth and (right column) sea ice thickness, in November 2018, (top) January 2019 (middle) and April 2019 (bottom) using rel004 data from strong beam 1 within an Inner Arctic Ocean domain for runs using snow depth/density from NESOSIM v1.0 (Nv1.0), v1.1 (Nv1.1) and the v1.1_2010-2020ave (Nv1.1c).

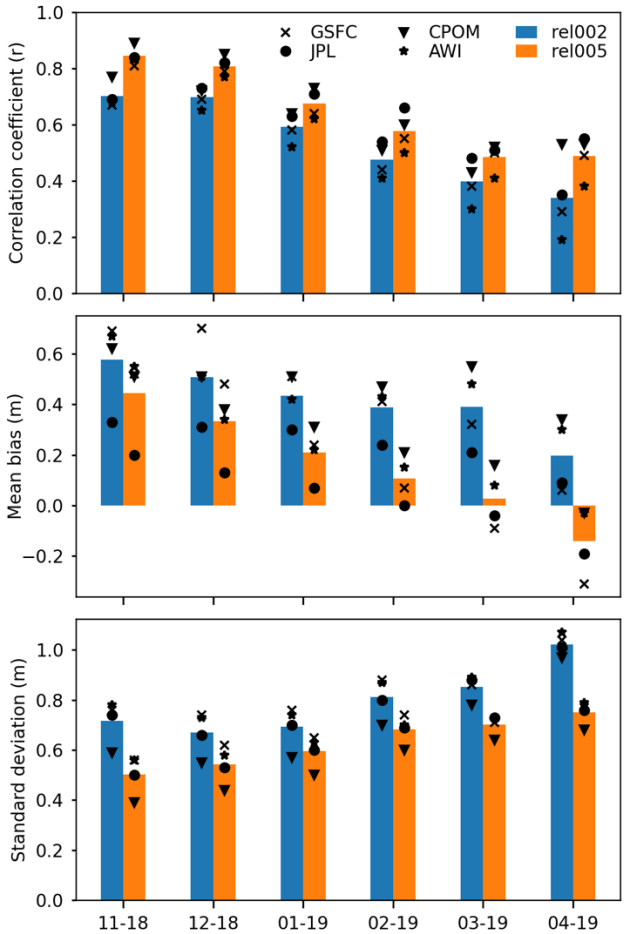

Figure 8: Comparison statistics of monthly gridded CryoSat-2 thickness for four different CryoSat-2 products (GSFC, JPL, CPOM, AWI) with monthly gridded ICESat-2 sea ice thickness using rel005 ATL10 and the same snow loading and ice density input assumptions from November 2018 (11-18) to April 2019 (04-19). Data are compared within our Inner Arctic Ocean domain and for grid-cells in both datasets that contain thicknesses > 0.25 m.

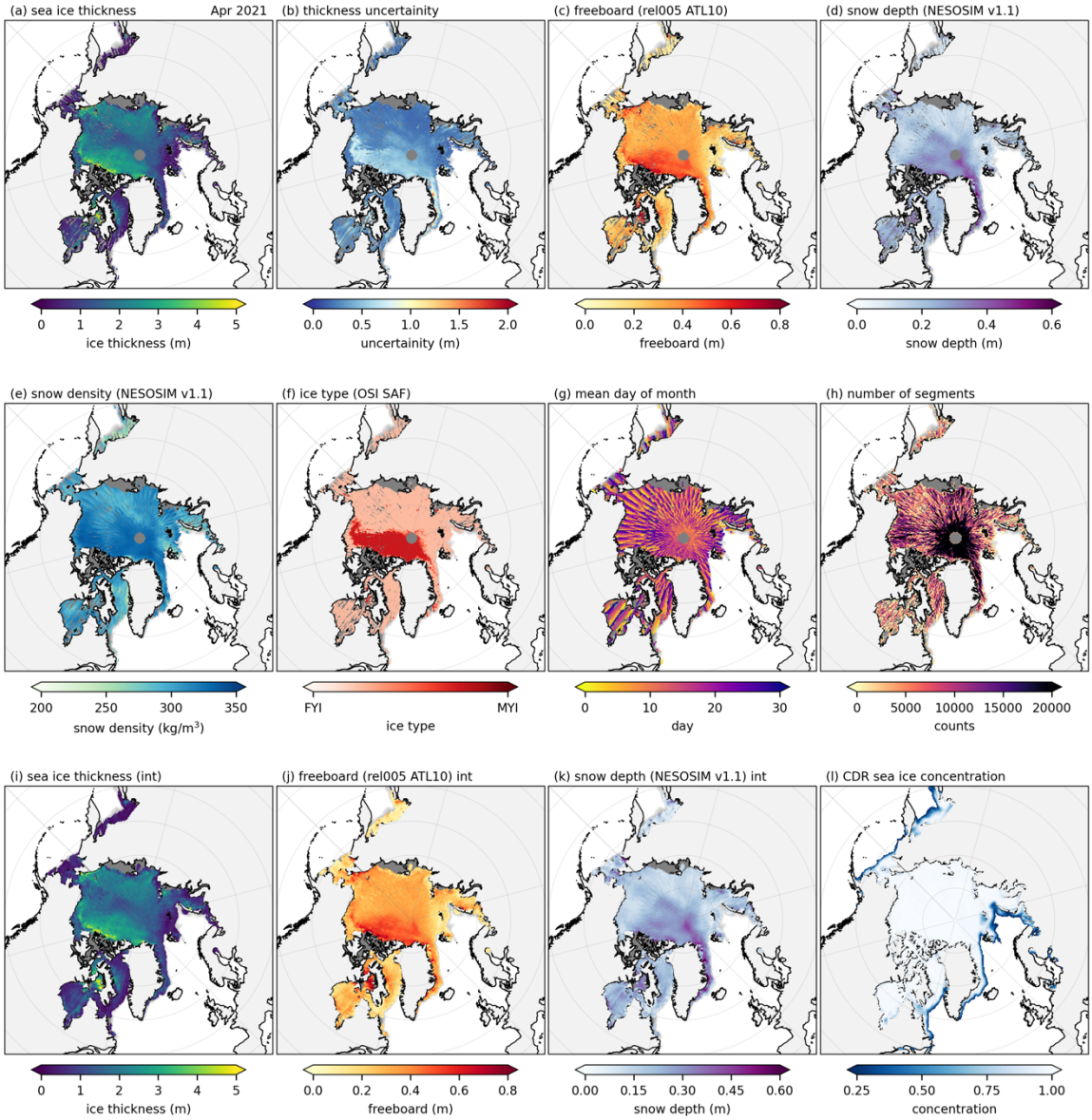

Figure 9: Example monthly gridded sea ice thickness dataset (IS2SITMOGR4, version 2) for April 2021. Dataset derived from rel005 ATL10 freeboards and NESOSIM v1.1 snow loading across all three strong beams. The background gray shading in panels a to k is the CDR sea ice concentration shown in panel i. Panels i to k show interpolated/smoothed variables.

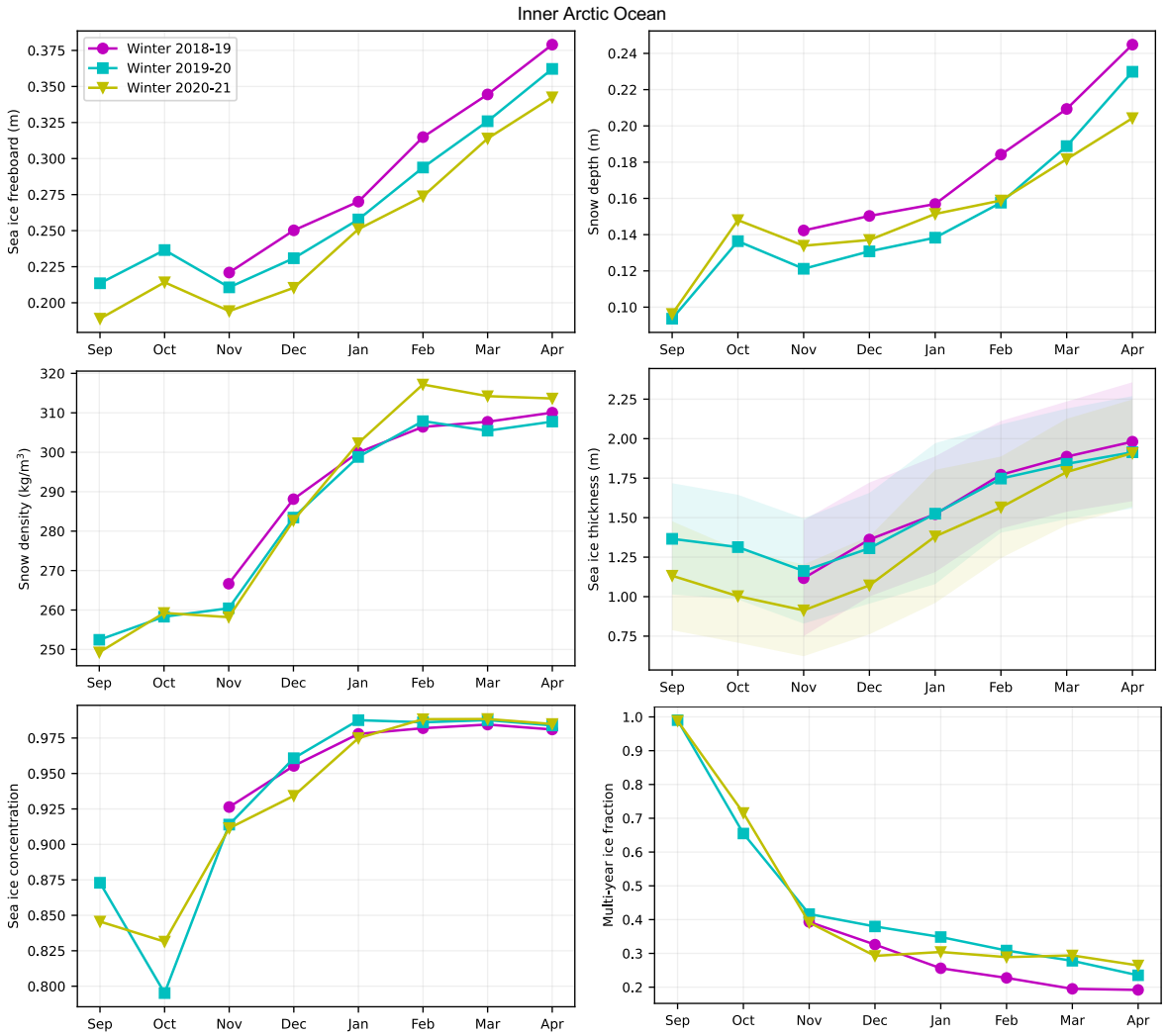

Figure 10: Time series of monthly mean ICESat-2 Inner Arctic Ocean sea ice freeboard (top left), redistributed NESOSIM v1.1 snow depth (top right), NESOSIM v1.1 snow density (middle left), OSI SAF multi-year ice fraction (middle right), CDR sea ice concentration (bottom left) and resultant sea ice thickness (bottom right) for the 2018/2019, 2019/2020 2020/2021 winters. Monthly means are generated using monthly gridded ICESat-2 thickness estimates (IS2SITMOGR4 v2, shown in Figure 8), masked outside of an Inner Arctic Ocean domain (see Figure S3). The shading in the lower right panel represents the mean systematic thickness uncertainty (see Figure 9b for an example monthly ice thickness uncertainty field).

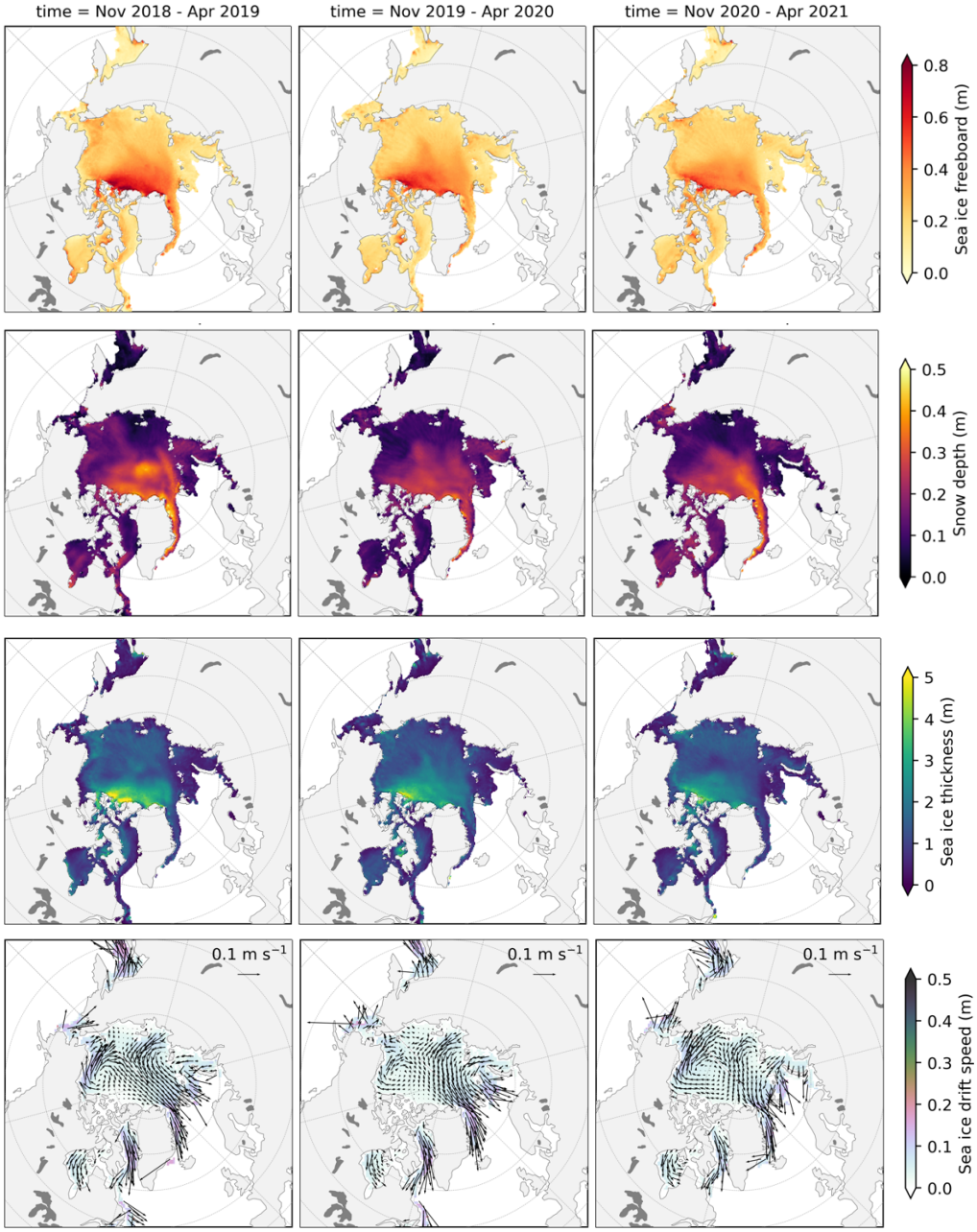

Figure 11: Winter (November to April) mean ICESat-2 freeboard (top) redistributed NESOSIM v1.1 snow depth (second row), sea ice thickness (third row) and OSI SAF sea ice drifts (bottom row) for the 2018-2019 (left column) 2019-2020

(middle column) and 2020-2021 (right column) winters based on the monthly gridded IS2SITMOGR4 v2 data (using the interpolated/smoothed variables for each variable). The thickness data are overlaid with winter mean OSI SAF drift vectors.

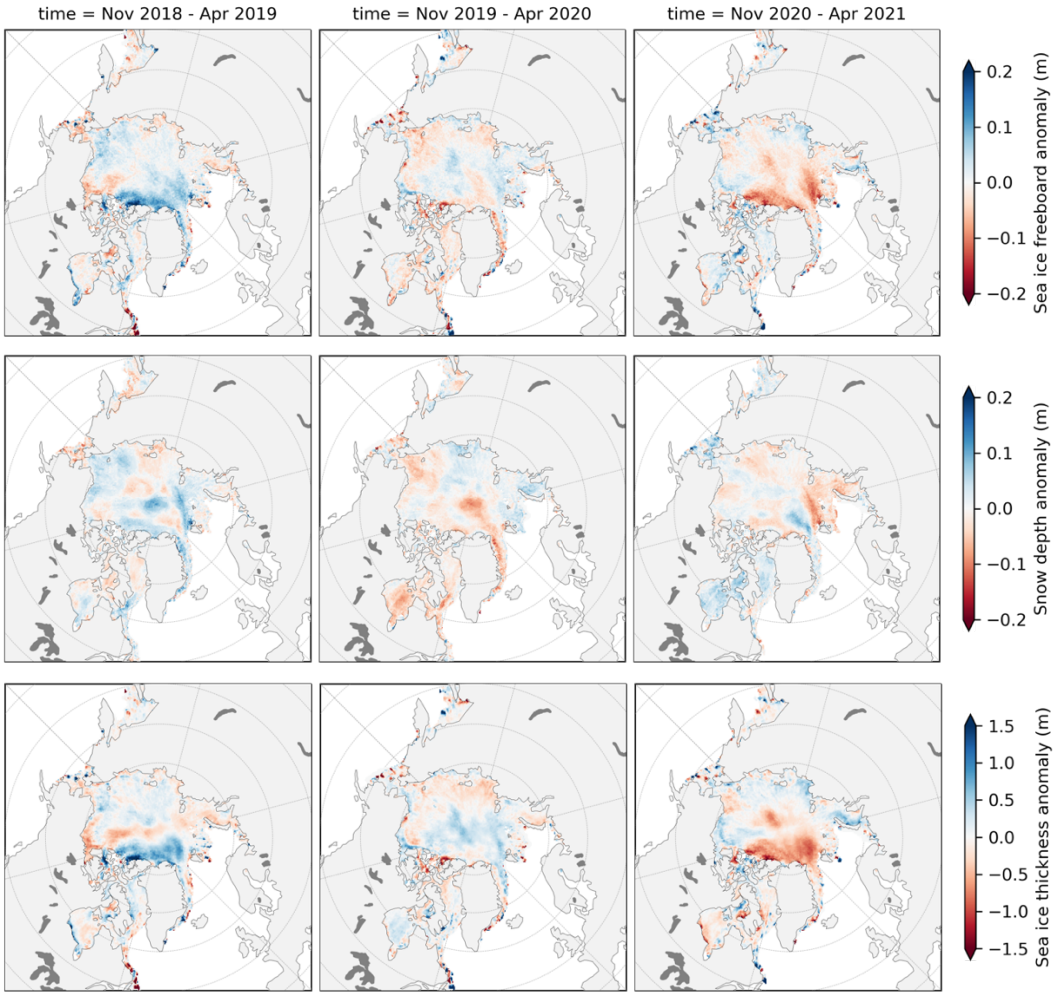

Figure 12: As in Figure 11 but showing the anomalies relative to the 2018-2021 winter means for the 2018-2019 (left column) 2019-2020 (middle column) and 2020-2021 (right column) winters.

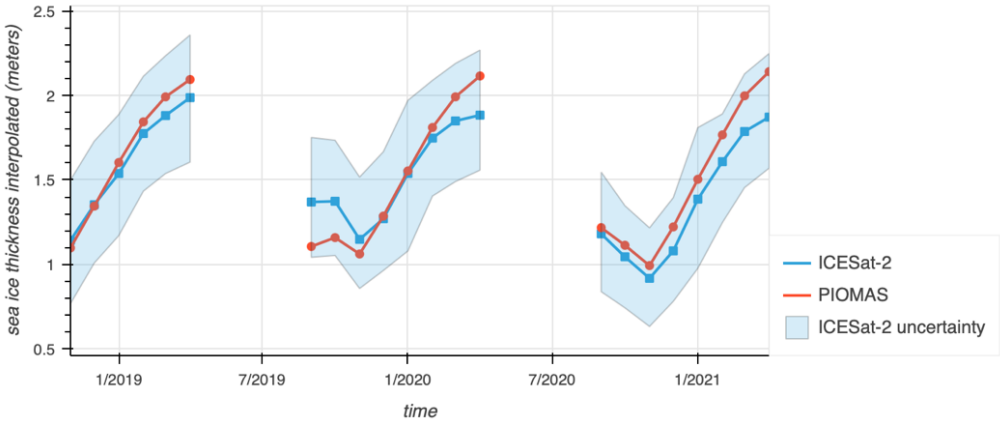

Figure 13: Comparisons of our monthly mean gridded ICESat-2-derived thickness estimates (IS2SITMOGR4, v002) against thickness estimates from PIOMAS. Data limited to >90% sea ice concentration within our Inner Arctic Ocean domain where both datasets provided positive (> 1 cm) thicknesses

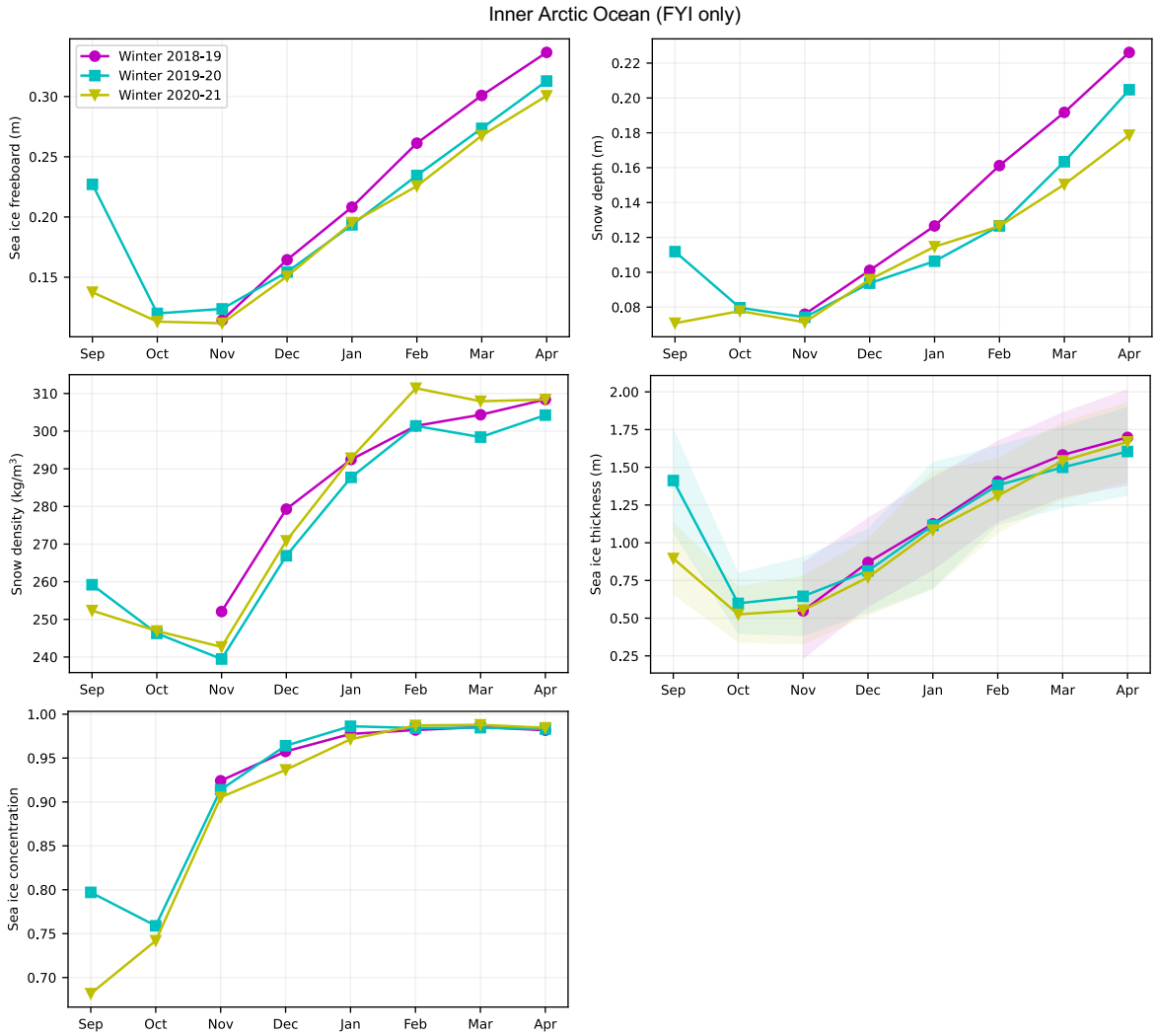

995 **Figure 14:** As in Figure 10 but for monthly means of grid-cells identified as first-year ice (FYI) only based on the OSI SAF ice type product.

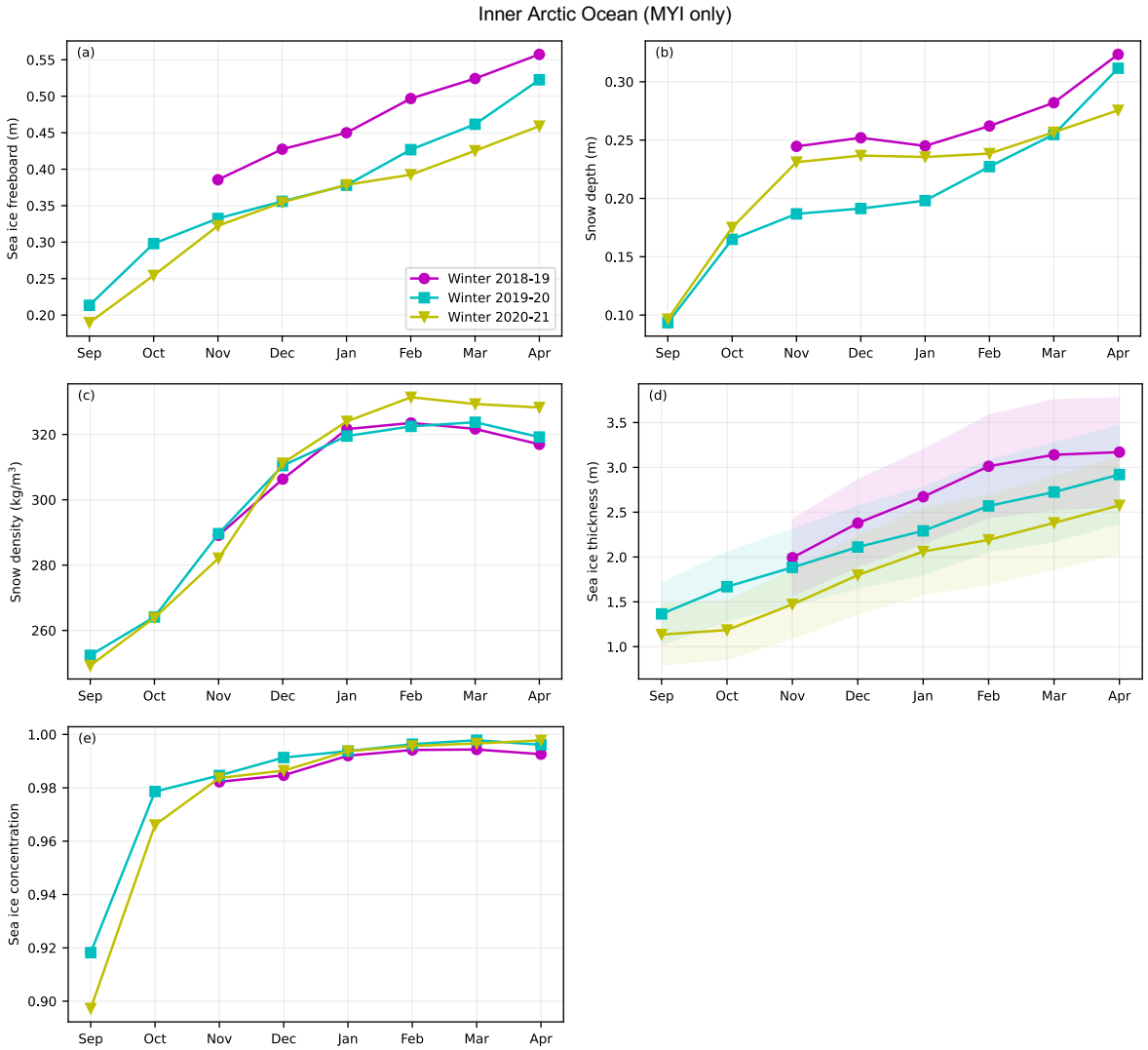

Figure 15: As in Figure 10 but for monthly means of grid-cells identified as multiyear ice (MYI) only based on the OSI SAF ice type product.

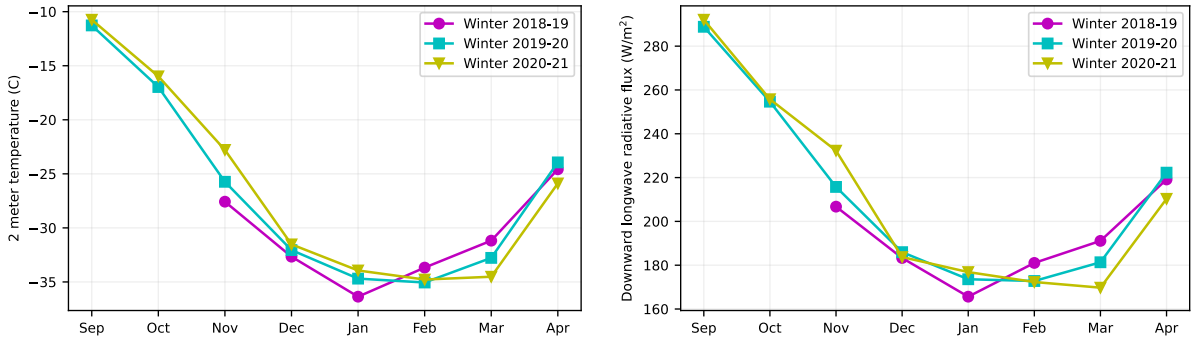

Figure 16: Time series of monthly mean 2 m temperature and downwelling longwave radiation from ERA5 within our Inner Arctic Ocean region.